



**NTNU – Trondheim**  
Norwegian University of  
Science and Technology

# Flow conditions in spiral casing and the influence of various bend geometries

**Tage Morken Augustson**

Mechanical Engineering

Submission date: June 2013

Supervisor: Torbjørn Kristian Nielsen, EPT

Norwegian University of Science and Technology  
Department of Energy and Process Engineering



# Oppgavetekst

## Bakgrunn og målsetting

Gjennom at EUs energidirektiv ble underskrevet har Norge og Sverige forpliktet seg til å bygge ut over 26 TWh fornybar energi. For å få fart på utbyggingen har Norge og Sverige innført såkalte elsertifikater. Elsertifikater tildeles også for økt energi-produksjon som følge av forbedring av eksisterende vannkraftverk. Dette innebærer at man må måle virkningsgraden både før og etter oppgradering av kraftverk. Måling av kraftverk med lave fallhøyder kan være problematisk både med tanke på økonomi og nøyaktighet.

I prosjektoppgaven har kandidaten undersøkt og beskrevet metoder for måling av virkningsgrader ved lave fallhøyder.

Under prosjektarbeidet har han diskutert påvirkning av hastighetsfordelingen inn mot turbinen. Det er av stor interesse, spesielt for lavtrykksturbiner, å se nærmere på hvordan vannveidesignene påvirker innløpsbetingelsen for turbinen og dermed påvirker virkningsgraden

## Oppgave bearbeides ut fra følgende punkter

1. Analysere hvordan skjevt hastighetsprofil kan gi årsak til lav virkningsgrad
2. Skaffe en oversikt over hvordan og i hvilken grad ulike rørbendgeometrier påvirker strømningsforhold og hastighetsfelt.
3. Simulere strømning gjennom en turbins spiraltromme og stagskovler hvor innløpsbetingelsene er definert av vannveien.
4. Planlegge gjennomføring av målinger

Oppgaven gitt: 14. januar 2013  
Hovedveileder: Torbjørn Kristian Nielsen, EPT

Senest 14 dager etter utlevering av oppgaven skal kandidaten levere/sende instituttet en detaljert fremdrift- og eventuelt forsøksplan for oppgaven til evaluering og eventuelt diskusjon med faglig ansvarlig/veiledere. Detaljer ved eventuell utførelse av dataprogrammer skal avtales nærmere i samråd med faglig ansvarlig.

Besvarelsen redigeres mest mulig som en forskningsrapport med et sammendrag både på norsk og engelsk, konklusjon, litteraturliste, innholdsfortegnelse etc. Ved utarbeidelsen av teksten skal kandidaten legge vekt på å gjøre teksten oversiktlig og velskrevet. Med henblikk på lesning av besvarelsen er det viktig at de nødvendige henvisninger for korresponderende steder i tekst, tabeller og figurer anføres på begge steder. Ved bedømmelsen legges det stor vekt på at resultatene er grundig bearbeidet, at de oppstilles tabellarisk og/eller grafisk på en oversiktlig måte, og at de er diskutert utførlig.

Alle benyttede kilder, også muntlige opplysninger, skal oppgis på fullstendig måte. For tidsskrifter og bøker oppgis forfatter, tittel, årgang, sidetall og eventuelt figurnummer.

Det forutsettes at kandidaten tar initiativ til og holder nødvendig kontakt med faglærer og veileder(e). Kandidaten skal rette seg etter de reglementer og retningslinjer som gjelder ved alle (andre) fagmiljøer som kandidaten har kontakt med gjennom sin utførelse av oppgaven, samt etter eventuelle pålegg fra Institutt for energi- og prosessteknikk.

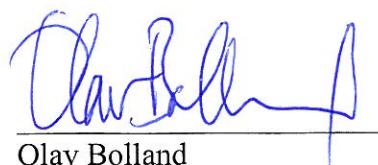
Risikovurdering av kandidatens arbeid skal gjennomføres i henhold til instituttets prosedyrer. Risikovurderingen skal dokumenteres og inngå som del av besvarelsen. Hendelser relatert til kandidatens arbeid med uheldig innvirkning på helse, miljø eller sikkerhet, skal dokumenteres og inngå som en del av besvarelsen. Hvis dokumentasjonen på risikovurderingen utgjør veldig mange sider, leveres den fulle versjonen elektronisk til veileder og et utdrag inkluderes i besvarelsen.

I henhold til "Utfyllende regler til studieforskriften for teknologistudiet/sivilingeniørstudiet" ved NTNU § 20, forbeholder instituttet seg retten til å benytte alle resultater og data til undervisnings- og forskningsformål, samt til fremtidige publikasjoner.


Besvarelsen leveres digitalt i DAIM. Et faglig sammendrag med oppgavens tittel, kandidatens navn, veileders navn, årstall, instituttnavn, og NTNUs logo og navn, leveres til instituttet som en separat pdf-fil. Etter avtale leveres besvarelse og evt. annet materiale til veileder i digitalt format.

- Arbeid i laboratorium (vannkraftlaboratoriet, strømnings teknisk, varmeteknisk)
- Feltarbeid

NTNU, Institutt for energi- og prosessteknikk, 14. januar 2013



Olav Bolland  
Instituttleder

  
Torbjørn K. Nielsen  
Faglig ansvarlig/veileder



# Problem description

## Background and goal

After the European Union directive called the “Renewables Directive” (2009/28/EC) was signed, Norway and Sweden have committed themselves to increase the renewable energy production by another 26 TWh. In order to stimulate this increased production, Norway and Sweden have implemented so-called “el-certificates”. El-certificates are also granted for the increased energy production following improvement of existing hydropower plants. This involves measuring efficiency both before and after upgrading the actual power plant. Carrying out measurements at low head power plants may be challenging both economically and with respect to the measurement accuracy.

During the specialization project, the candidate investigated and described methods for efficiency measurements at low head power plants.

During the author's specialization project (Augustson, 2012), the effect of bends on velocity profiles, and the importance of the velocity distribution at the inlet of turbines, were briefly discussed. It is of great interest, especially concerning low head turbines, to look closer into how conduit designers affect the inlet conditions of the turbine, and hence the turbine efficiency.

## Work description

1. Analyse how skewed velocity profiles may cause low efficiency.
2. Get an overview of how and to which extent various bend geometries affect flow conditions and velocity fields.
3. Simulate the flow through a spiral casing including stay vanes, using flow conditions determined by the conduit geometry.
4. Plan execution of measurements

Task given: January 14, 2013

Supervisor: Torbjørn Kristian Nielsen, EPT



# Preface

The work with this thesis has to a large extent been focused on applying CFD software for prediction of fluid flow behaviour in various geometries. This has been a very interesting journey which has allowed me to gain a great deal of experience using various CFD software like OpenFOAM and ANSYS, and I am very grateful for this. Therefore I would like to thank my supervisor Torbjørn Nielsen for assigning me such an interesting topic, and allowing me to go deeper into a field of hydropower flow analysis that I find very exciting.

Although CFD software may yield very interesting and useful results, making them work in the desired way may be a time-consuming and difficult process. I would like to give a special thanks to Bjørn Winther Solemslie for helping me in the process of preparing the design model and introducing me to CFX.

Thanks also to my fellow students Kjartan Furnes and Jone Rivrud Rygg, who were also working on CFD related subjects. Kjartan, for his valuable insights into computing and post-processing, and Jone, for going deep into the various meshing strategies applicable to OpenFOAM and ANSYS.

Last but not least, thanks to fellow student Julie Marie Hovland, for supplying me with her nicely made Paint drawing in Figure 8.1.

*Tage M. Augustson*

Tage Morken Augustson  
Trondheim, April 29, 2013





# Sammendrag

Både tidligere eksperimenter og CFD-simuleringer viser at bend har betydelig innvirkning på hastighetsfeltet nedstrøms, spesielt ved å danne såkalte «skjeve hastighetsprofiler». Basert på simuleringene utført i OpenFOAM under arbeidet med denne oppgaven, har de aksielle hastighetsprofilene nedstrøms bend med utvalgte geometrier blitt plottet, og beskrevet i mer detalj enn forfatteren har kunnet finne i tidligere arbeider. Funnene ble delt inn i karakteristikk for hastighetsprofiler i «Plan AA» og Plan BB», som er definert i Figur 2.1, mens bend-simuleringene ble utført på fire ulike bendgeometrier med to ulike vinkler og to ulike relative radier, som er oppsummert i Tabell 4.1.

Generelt sett ble det observert at større bendvinkler og mindre relativ radius medførte større skjevhet i hastighetsprofilene. Bend med små relative radier har ofte skarpere konvekative hastighetsgradienter, dvs. større endring i hastighet over posisjon, spesielt like etter utløpet av bendet.

Ved 45-gradersbend (relativt liten bendvinkel), ser innflytelsen av å bruke ulike relative radier (f. eks.  $R/r=2$  vs.  $R/r=8$ ) ut til å ha mindre innvirkning på hastighetsfeltets skjevhet enn den har ved 90-gradersbend.

En rekke simuleringer ble utført på et mesh av NTNUs Tokke-spiraltrømme-modell, ved bruk av ANSYS til meshing og CFX til simulering og post-prosessering. Radielle hastighetsprofiler ved utløpet av stagskoblene ble plottet mot den vinkelbaserte posisjonen ved utløpet. Som ventet, gjorde de 14 stagskoblene at hastighetsprofilen ble delt opp i 14 «topper» (se Figur 5.4.3.2a og b), hver tilsvarende en av de 14 stagskoblkanalene som vannet passerer gjennom på vei mot ledeskoblene, og tilslutt inn i løpehullet. Basert på plott av radielle hastighetskomponenter, ser det ut til at det oppstår en generell form på hvert hastighetsprofil, som ser ut som en enkel, skjev, «hoggtann-formet» topp. Hoggtann-formen til hvert hastighetsprofil skyldes en skjevhet mot *innsiden* av kanal-kurvaturen, der gradienten til den radielle hastigheten over vinkelbasert posisjon ( $\frac{\partial u_r}{\partial \theta}$ ) er større på innsiden av kanalkurvaturen enn utsiden.

Dette fenomenet er veldig likt det skjeve hastighetsprofilen i Plan AA, som oppstår like etter at et hastighetsfelt passerer innløpet til et bend, før det skifter side og heller mot siden som tilsvarer *utsiden* av bendkurvaturen.

Selv om spiraltrømme- og stagskobl-designet til Tokke-spiraltrømme-modellen oppnår lignende radielle hastighetsprofiler fra hver kanal, varierer hastighetenes størrelser, og dermed volumstrømmen, gjennom hver kanal mer enn det som antageligvis er optimalt. F. eks. har peak-hastighetene gjennom første og siste kanal, som er kanalene med henholdsvis høyest og lavest peak-hastighet, et absolutt peak-hastighetsforskjell på 25%.

# Abstract

Both previous experiments and CFD simulations show that bends have a significant influence on the downstream flow field, especially by causing so-called “skewed velocity profiles”. Based on the simulations carried out in OpenFOAM during this thesis, the axial velocity profiles downstream of bends of a few selected geometries have been plotted and described in more detail than what the author has managed to find in previous work. The findings were divided into characteristics of velocity profiles in “Plane AA” and “Plane BB”, which are defined in Figure 2.1, while the bend simulations were carried out on four different bend geometries of two different angles and two different relative radiuses, which are listed in Table 4.1.

In general, it was found that a sharper bend angle and a smaller relative radius lead to more skewness in the velocity profiles. Bends with small relative radiuses also tend to have sharper convective velocity gradients, i.e. sharper change in velocity over change in position, especially shortly after the outlet of the bend.

In the case of the 45 degree bend (relatively small bend angle), the influence of using various relative radiuses (e.g.  $R/r=2$  vs.  $R/r=8$ ) seemed to make less impact on the velocity field skewness than that of the 90 degree bend.

A number of simulations were carried out on a mesh of the NTNU Tokke spiral casing model, using ANSYS for meshing and CFX for simulation and post-processing. Radial velocity profiles at the outlet of the stay vanes were plotted against the angular position at the outlet. As expected due to the effect of the 14 stay vanes on the velocity distribution, the velocity field appeared divided into 14 velocity profile “peaks” (see Figure 5.4.3.2a and b), each corresponding to one of the 14 stay vane channels that the water passes through on its way towards the guide vanes, and eventually into the runner.

Based on the plots of the radial velocity components, it appears that the general shape of each velocity profile looks like a single, skewed and “fang-shaped” peak. The fang-shape of each profile is caused by a skewness leaning towards the *inner* curve of the channel curvature, where the gradient of the radial velocity over angular location ( $\frac{\partial u_r}{\partial \theta}$ ) is larger at the inner part of the channel than at the outer part. This phenomenon is very similar to the skewed velocity profile in Plane AA that occurs shortly after a flow field enters the inlet of a bend, before it switches and starts skewing towards the side corresponding to the *outer* curve of the bend curvature.

Although the spiral casing and stay vane design of the Tokke spiral casing model successfully achieves similar radial velocity profile shapes from each channel, the magnitude of the velocities, and thus the volumetric flow, going through each channel, varies more than what should be optimal. E.g., the peak velocities going through the first and the last channel, which are the channels with the lowest and highest peak velocity, respectively, have an absolute velocity difference of about 25%.

# Contents

Preface.....	iv
Sammendrag.....	vi
Abstract .....	vii
List of Figures .....	xii
List of Tables.....	xiv
Nomenclature .....	xv
1 Introduction.....	1
2 Background theory .....	3
2.1 Pressure losses in pipe flows.....	3
2.2 Turbulent velocity profiles in straight pipes .....	4
2.2.1 Entrance length of turbulent pipe flow .....	4
2.2.2 The logarithmic overlap-law .....	4
2.2.3 The power-law .....	5
2.3 Axial velocity profiles in curved pipes .....	6
2.4 Runner inlet velocities .....	8
2.5 Using OpenFOAM.....	9
2.5.1 Handling the kinematic pressure values given by OpenFOAM ..	9
2.5.2 Estimating the parameters $k$ and $\varepsilon$ of the $k$ - $\varepsilon$ model.....	9
3 Relevant previous work .....	12
3.1 “Analysis of flow in the spiral casing using a streamline upwind Petrov Galerkin method” .....	12
3.2 “Assessment of turbulence modelling for CFD simulations into hydroturbines: Spiral casings” .....	13
3.3 “Structure- and fluide-borne acoustic power sources induced by turbulent flow in 90° piping elbows” .....	14
4 Bend simulations using OpenFOAM.....	15
4.1 Definition of geometries .....	15
4.2 Pre-processing in OpenFOAM.....	16

4.2.1	Defining number of cells.....	16
4.2.2	Defining boundary conditions.....	16
4.3	Post-processing using ParaView .....	18
4.3.1	Creating Slice views as used in Chapter 4.4.1 .....	18
4.3.2	Plotting velocity profiles as used in Chapter 4.4.2 .....	19
4.4	Results from bend simulations.....	20
4.4.1	Pressure and velocity fields in bends .....	20
4.4.1.1	45 degree bend with relative radius $R/r=2$ .....	20
4.4.1.2	45 degree bend with relative radius $R/r=8$ .....	20
4.4.1.3	90 degree bend with relative radius $R/r=2$ .....	21
4.4.1.4	90 degree bend with relative radius $R/r=8$ .....	21
4.4.2	Axial velocity profiles downstream of various bend geometries ..	22
4.4.2.1	45 degree bend with relative radius $R/r=2$ .....	23
4.4.2.2	45 degree bend with relative radius $R/r=8$ .....	23
4.4.2.3	90 degree bend with relative radius $R/r=2$ .....	23
4.4.2.4	90 degree bend with relative radius $R/r=8$ .....	24
4.4.3	Axial velocity components plotted against axial distance downstream of various bend geometries.....	25
4.4.3.1	45 degree bend with relative radius $R/r=2$ .....	26
4.4.3.2	45 degree bend with relative radius $R/r=8$ .....	26
4.4.3.3	90 degree bend with relative radius $R/r=2$ .....	27
4.4.3.4	90 degree bend with relative radius $R/r=8$ .....	27
5	Spiral casing simulations using CFX.....	28
5.1	Definition and preparation of geometry.....	28
5.2	Pre-processing in ANSYS.....	29
5.2.1	Meshing in ANSYS.....	29
5.2.2	Defining boundary conditions in CFX.....	29
5.3	Post-processing in CFX .....	31
5.3.1	Colour plot of the flow field inside the spiral casing.....	31
5.3.2	Radial velocity plotted along the outlet of the spiral casing.....	32
5.4	Results from spiral casing simulations.....	34

5.4.1	Velocity fields in horizontal plane .....	34
5.4.2	Pressure fields in horizontal plane .....	35
5.4.3	Streamlines below horizontal plane, with spiral casing surface ..	35
5.4.3	Radial velocity at the outlet of the spiral casing .....	36
6	Discussion .....	39
6.1	Possible consequences of skewness and secondary flows at the spiral casing inlet .....	39
6.2	Reasons for simulating penstock and bend geometries isolated from spiral casing.....	39
7	Conclusions.....	41
7.1	Undesirable effects of poor velocity distribution at the inlet of a runner	41
7.2	The influence of bends on flow conditions .....	41
	Bibliography.....	43
	Appendix A: Calculations involved in a bend mesh creator for OpenFOAM's blockMeshDict .....	49
	Introduction.....	49
	The placement of the mesh in the coordinate system .....	50
	Calculating vertice coordinates .....	50
	Setting blocks .....	51
	Calculating arc coordinates .....	51



# List of Figures

## Chapter 2

Figure 2.3.1 [3]: Illustration of the location of Plane AA and Plane BB .....	6
Figure 2.3.2 [3]: Simulated (lines) and experimental (dots) data for axial velocity through a bend .....	7
Figure 2.4 [11]: Velocity components in a Francis turbine.....	8

## Chapter 3

Figure 3.1.1 [7]: Mesh for the spiral casing, which appears to have been modeled without stay vanes. ....	12
Figure 3.1.2 [7]: Average flow characteristics at the outlet of the spiral casing, as a function of the angular location (polar angle) .....	12
Figure 3.2.1 [8]: Full overview of a simulated mesh, with a 90 degree bend located in close vicinity of the cake-shaped spiral casing.....	13
Figure 3.2.2 [8]: A close look at the mesh surrounding the stay and guide vanes, which appear as black, droplet-shaped holes in the mesh .....	13
Figure 3.2.3 [8]: The location of the measured cross-section, seen from above .....	13
Figure 3.2.4 [8]: A vertical cross-section of the left side of the Kaplan spiral casing and runner, with the measured cross-section coloured in green.....	13
Figure 3.3.1 [9]: Slices showing secondary flow pattern at outlet of pipe bend .....	14
Figure 3.3.2 [9]: Slices of velocity magnitude through and downstream of a 90 degree pipe bend .....	14
Figure 3.3.3 [9]: Velocity profile, plotted in red, in the fully develop region upstream of the pipe bend.....	14
Figure 3.3.4 [9]: Velocity profile, plotted in red, near the exit of the computational domain downstream of the pipe bend.....	14

## Chapter 4

Figure 4.1.1: Geometry I .....	15
Figure 4.1.2: Geometry II .....	15
Figure 4.1.3: Geometry III .....	15
Figure 4.1.4: Geometry IV .....	15
Figure 4.3.1: There is also a Slice button available in one of the upper toolbars .....	18
Figure 4.3.2: Locations of the drop-down lists “Filters” and “Solid Color”, the tabs “Properties” and “Display”, and the variables “p” and “U (Magnitude)” .....	19
Figure 4.4.1.1a: Pressure field.....	20
Figure 4.4.1.1b: Velocity field.....	20
Figure 4.4.1.2a: Pressure field.....	20
Figure 4.4.1.2b: Velocity field.....	20
Figure 4.4.1.3a: Pressure field.....	21
Figure 4.4.1.3b: Velocity field.....	21
Figure 4.4.1.4a: Pressure field.....	21



Figure 4.4.1.4b: Velocity field .....	21
Figure 4.4.2.1a: Plane AA .....	23
Figure 4.4.2.1b: Plane BB .....	23
Figure 4.4.2.2a: Plane AA .....	23
Figure 4.4.2.2b: Plane BB .....	23
Figure 4.4.2.3a: Plane AA .....	24
Figure 4.4.2.3b: Plane BB.....	24
Figure 4.4.2.4a: Plane AA .....	24
Figure 4.4.2.4b: Plane BB .....	24
Figure 4.4.3: The location of the various velocity components plotted on the following two pages, defined in the YZ plane, relative to the pipe walls .....	25

Figure 4.4.3.1: When dealing with a 45 degree bend with R/r=2, the convective acceleration $\frac{\delta u}{\delta x} = 0$ at $x/D \approx 12.6$ for the “Center” velocity component.....	26
Figure 4.4.3.2: When dealing with a 45 degree bend with R/r=8, the convective acceleration $\frac{\delta u}{\delta x} = 0$ at $x/D \approx 13.4$ for the “Center” velocity component.....	26
Figure 4.4.3.3: When dealing with a 90 degree bend with R/r=2, the convective acceleration $\frac{\delta u}{\delta x} = 0$ at $x/D \approx 5.5$ for the “Center” velocity component.....	27
Figure 4.4.3.4: When dealing with a 90 degree bend with R/r=2, the convective acceleration $\frac{\delta u}{\delta x} = 0$ at $x/D \approx 7.0$ for the “Center” velocity component.....	27

**Chapter 5**

Figure 5.1: The internal flow volume of the Tokke spiral casing model, meshed in ANSYS .....	28
Figure 5.2: What the model should look like in CFX-Pre after defining Inlet and Outlet boundaries.....	30
Figure 5.3: This figure should show up after applying “Volume Rendering” for Velocity and using a “Clip Plane” in CFX-Post.....	31
Figure 5.4.1a: 1 641 075-cell mesh .....	34
Figure 5.4.1b: 5 127 891-cell mesh .....	34
Figure 5.4.2a: 1 641 075-cell mesh .....	35
Figure 5.4.2b: 5 127 891-cell mesh .....	35
Figure 5.4.3a: 1 641 075-cell mesh .....	35
Figure 5.4.3b: 5 127 891-cell mesh .....	35
Figure 5.4.3.1: The definition of the angular location, which is being referred to on the following pages .....	36
Figure 5.4.3.2a: Resulting radial velocities from a simulation with a 1 641 075-cell	

mesh and an inlet velocity of 3.5355 m/s .....	37
Figure 5.4.3.2b: Resulting radial velocities from a simulation with a 5 127 891-cell mesh and an inlet velocity of 2.8645 m/s .....	37

## List of Tables

Table 4.1: Parameters of simulated geometries .....	15
Table 4.2: Boundary conditions at the various patches .....	17

# Nomenclature

## Latin symbols

$A$	Near universal constant for outer velocity profile	
$B$	Near-universal constant for inner velocity profile	
$C$	Coefficient of the power-law overlap formula; constant $C_\mu \approx 0.09$ for estimating turbulent dissipation rate	
$c$	Absolute water velocity	$m/s$
$d$	Hydraulic diameter	$m$
$f$	Darcy friction factor	
$g$	Gravitational acceleration	$m/s^2$
$h$	Pipe head loss	$m$
$k$	Turbulent kinetic energy	$m^2/s^2$
$l$	Turbulent length scale	$m$
$L$	Pipe length	$m$
$V$	Average flow velocity	$m/s$
$p$	Pressure	$Pa$
$P$	Kinematic pressure	$m^2/s^2$
$Re_D$	Reynolds number, $Vd/\nu$	
$T$	Turbulence intensity	
$u$	Local velocity $\bar{u}$ ; wall-friction velocity $u^*$ ; tangential velocity $u_2$ of runner; velocity fluctuations $u'$ ; mean flow velocity $u_{avg}$	$m/s$
$U$	Stream velocity $U_e$ ; mean flow velocity $U_{ref}$	$m/s$
$y$	Distance perpendicular to the wall	$m$

### Greek symbols

$\alpha$	The exponent of the power-law overlap formula	
$\Delta$	Difference/loss ( $\Delta p$ = Pressure loss)	
$\delta$	Velocity boundary-layer thickness	$m$
$\epsilon$	Turbulent dissipation rate	$W/kg$
$\kappa$	Kármán constant ( $\approx 0.41$ )	
$\nu$	Kinematic viscosity	$m^2/s$
$\rho$	Density	$kg/m^3$

### Subscripts

avg	Average value (e.g. average flow velocity $u_{avg}$ )
$D$	Stating that the Reynolds number $Re_D$ is based on the pipe diameter
$f$	Caused by friction (e.g. the pipe head loss $h_f$ )
$i$	Related to intensity (e.g. turbulence intensity $T_i$ )
$\mu$	Separates the dissipation rate constant $C_\mu \approx 0.09$ from the power-law coefficient $C$
2	Used in Chapter 2.4 to denote flow characteristics at the inlet of a runner

### Superscripts

—	Time-average (e.g. time-averaged local velocity $\bar{u}$ )
*	Used to separate friction velocity $u^*$ from local velocity $\bar{u}$
+	Used to specify that $u^+$ and $y^+$ specify dimensionless velocity and distance, respectively
*	Used to specify that $*c_2$ is the ideal water flow velocity.
'	Separates the root-mean-square $u'$ of the velocity fluctuations from other forms of velocity $u$ .

# 1 Introduction

The hydraulic efficiency of a hydro power plant is a measure of how well the power plant is able to transfer the potential energy of the water to mechanical energy in the runner. Two important causes of reduced hydraulic efficiency, or hydraulic losses, in a power plant may typically be:

1. Losses upstream of the turbine, due to wall friction, trash racks, valves, bends etc.
2. Inefficient flow conditions in the spiral casing and runner, e.g. swirls, strong secondary flows and non-uniform velocity distribution at the runner inlet.

Identifying the right causes of hydraulic losses is of great importance both when it comes to making good decisions concerning operation and maintenance, as well as concerning the actual power plant and turbine design. The ability of identifying the causes of hydraulic losses will usually depend on a combination of making the right measurements at the right places, and an accurate understanding of what is likely to be the cause of the losses in each specific case. There is currently a wide range of empirical loss factors and equations available on how to calculate to expected hydraulic losses, caused by e.g.:

- Wall friction: the Moody diagram with the Darcy-Weisbach equation
- Trash racks: flow angle and rack design dependent loss-factors with Kirschmer's equation
- Valves and bends: various empirical loss factors with the Darcy-Weisbach equation

However, as these empirical relations are typically based on simple assumptions and ideal cases, they may not always be sufficient to predict accurately how a more complex system of factors may interact in an actual hydro power plant. Some examples are the losses caused by a valve designs which have not yet been subject to extensive empirical testing, or the combination of two or more consecutive bends, where the skewed velocity field created by the first bend may cause unexpected phenomena as it passes through the second one. These are examples of cases where computational fluid dynamics (CFD) may represent a good and useful alternative to laboratory experiments, which may not always be feasible or practical to carry out.

Considering the fact that the vast majority of hydro power plants with a spiral casing installed will also have a bend placed somewhere upstream of the actual spiral casing, makes the influence of this bend on the flow conditions developing through the spiral casing an interesting and potentially useful field of study, when it comes to further understanding the factors determining the hydraulic efficiency of a hydro power plant.

## 2 Background theory

### 2.1 Pressure losses in pipe flows

The Darcy-Weisbach applies to duct flows of any cross-section, and for laminar and turbulent flows. It gives a very useful relationship between the pipe head loss  $h_f$ , the Darcy friction factor  $f$ , the actual pipe length  $L$ , the pipe diameter  $d$ , the average flow velocity  $V$  and the gravitational acceleration  $g$ , and is written as follows (White, 2001, p. 340):

$$h_f = f \frac{L V^2}{d 2g} \quad (2.1)$$

Head loss  $h_f$  may also be expressed in terms of pressure loss  $\Delta p$ , by the equation (White, 2001, p. 345):

$$\Delta p = \rho g h_f \quad (2.2)$$

where  $\rho$  is the density of the water. Thus, a practical way of expressing pressure loss is given by combining Eq. (2.1) and (2.2):

$$\Delta p = \rho g h_f = \rho f \frac{L V^2}{d 2} \quad (2.3)$$

## 2.2 Turbulent velocity profiles in straight pipes

The following subchapters will summarize some important relationships occurring in turbulent pipe flows. Similar relationships exist for the entrance length and velocity profiles of laminar pipe flows, but these are not treated here as they are not considered relevant for this report.

### 2.2.1 Entrance length of turbulent pipe flow

According to an approximation for smooth walls, the entrance length  $L_e$  is given by the relation [1]:

$$\frac{L_e}{d} \approx 4.4Re_d^{1/6} \quad (2.4)$$

where  $d$  is the pipe diameter and  $Re_d$  is the Reynolds number.

### 2.2.2 The logarithmic overlap-law

According to the logarithmic overlap-law there are two equations suited to describe the shape of velocity profiles relative to smooth, impermeable walls [2]:

Inner variables: 
$$\frac{\bar{u}}{u^*} = \frac{1}{\kappa} \ln \frac{yu^*}{\nu} + B \quad (2.5)$$

Outer variables: 
$$\frac{U_e - \bar{u}}{u^*} = -\frac{1}{\kappa} \ln \frac{y}{\delta} + A \quad (2.6)$$

which include the local velocity  $\bar{u}$ , the wall-friction velocity  $u^*$ , the distance  $y$  perpendicular to the wall, the kinematic viscosity  $\nu$ , the stream velocity  $U_e$ , velocity boundary-layer thickness  $\delta$ , the near-universal constants  $\kappa \approx 0.41$  and  $B \approx 5.0$ , and the pressure gradient-dependent (and possibly other parameter-dependent) constant  $A$ .



### 2.2.3 The power-law

A new non-logarithmic formula has been proposed for the overlap law. This alternative overlap formula is proposed for both pipe flow and flat-plate flow, and relates the dimensionless flow velocity  $u^+$  to the Reynolds-dependent constants  $C$  and  $\alpha$ , and the dimensionless distance from the wall  $y^+$ , by the following equation [2]:

$$u^+ \approx C(y^+)^{\alpha} \quad (2.7)$$

The constants  $C$  and  $\alpha$  are acknowledged to vary with the Reynolds number  $Re_{\theta}$ , as follows:

$$C \approx 3 + 0.62\ln(Re_{\theta}) \quad \text{and} \quad \alpha \approx \frac{1.24}{\ln(Re_{\theta})} \quad (2.8)$$

## 2.3 Axial velocity profiles in curved pipes

To the author's knowledge, there are currently no simple analytical solutions describing turbulent velocity profiles in curved pipes, which do not involve solving the Navier-Stokes equation numerically on a larger flow field. However, there are plenty of experimental data and numerical analyses available, and a selection of these is listed in the following subchapters.

### 2.3.1. Definition of “Plane AA” and “Plane BB”

Before presenting the velocity profiles that tend to occur in turbulent pipe flows, it is useful to define the location of the lines for which these velocities will be plotted. This is illustrated by Figure 1, which shows that “Plane AA” is the line lying parallel to the radial direction of the bend curvature. “Plane BB”, on the other hand, is perpendicular to both “Plane AA” and the axial direction of the pipe, but parallel to the bend's axis of rotation.

It is useful to note that “Plane AA” and “Plane BB” will be referring to one-dimensional lines at which the velocity vectors are plotted, and not planes in the sense of two-dimensional surfaces. The author has chosen to refer to these two lines as “Plane” because this is what they were referred to in the paper *Prediction of turbulent flow in curved pipes* [3] by Patankar, Pratap and Spalding (1974).

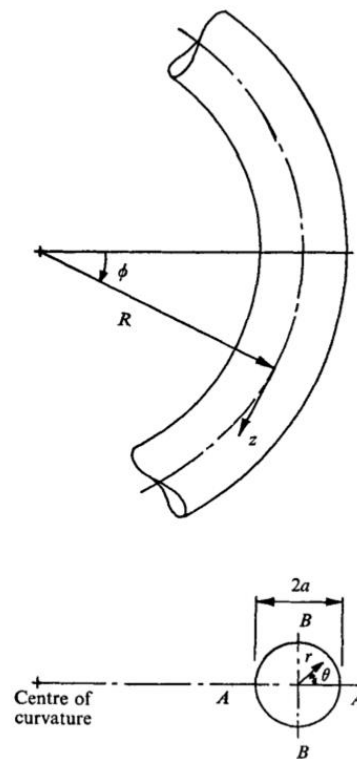


Figure 2.3.1 [3]: Illustration of the location of Plane AA and Plane BB

### 2.3.2 Axial velocity profiles in Plane AA and Plane BB

Figure 2 illustrates both simulated and experimental data for fully-developed axial velocity profiles in Plane AA and BB of a flow with a Reynolds number  $Re=8.9 \cdot 10^4$  and a relative radius  $R/a=25.9$ . The simulated data was found by Patankar, Pratap and Spalding [3] using the  $k-\varepsilon$  model.

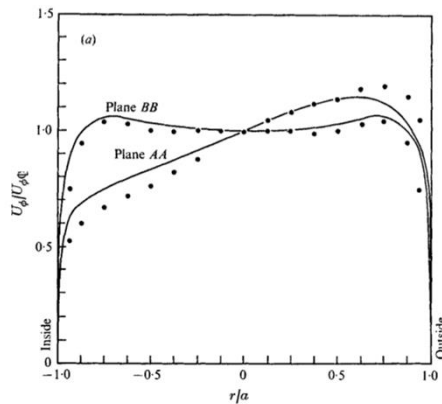


Figure 2.3.2 [3]: Simulated (lines) and experimental (dots) data for axial velocity through a bend

The simulated and experimental data correspond well, suggesting that the  $k-\varepsilon$  model yields acceptable results for this type of simulations.

## 2.4 Runner inlet velocities

Figure 2 shows how the direction of the absolute velocity  $c_2$  of the water flowing towards the runner is described by the angle  $\alpha_2$ , and that the direction  $\beta_2$  of the relative velocity into the runner is set by the design of the runner. Furthermore, the absolute tangential velocity  $u_2$  of the runner is restricted by the rotational velocity of the runner. When assuming that all the parameters  $\alpha_2$ ,  $\beta_2$  and  $u_2$  are fixed, then there should be an ideal value (which we will refer to as  $*c_2$ ) of our absolute velocity  $c_2$  of the water.

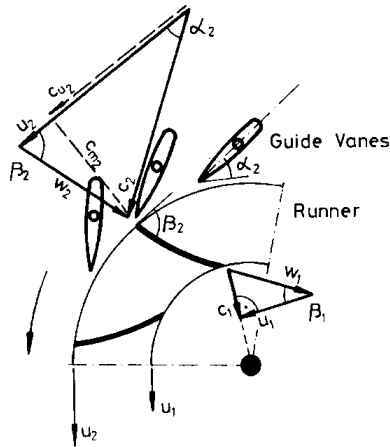


Figure 2.4 [11]: Velocity components in a Francis turbine

If we imagine that  $c_2$  at any given side of the runner inlet is higher than  $*c_2$ , then the immediate effect of this is likely to be an increased pressure at the pressure side of the actual blade channel. On the contrary, if  $c_2 < *c_2$ , then the effect is likely to be opposite: a decreased pressure on the pressure side of the blade channel, and increased pressure on the suction side. Since  $c_2 < *c_2$  implies that the flow moves slower than the blades it ought to pass, the effect will eventually be that the water starts extracting energy from the runner, rather than transferring it.

In other words, an evenly distributed velocity field at the inlet of the Francis runner should be ideal in terms of hydraulic efficiency. Consequently, this becomes an important parameter for spiral casing design. In fact, literature states that the spiral casing of a Francis turbine is designed such that the velocity distribution in the circumferential area of the inlet to the stay vanes is uniform. [10]

## 2.5 Using OpenFOAM

### 2.5.1 Handling the kinematic pressure values given by OpenFOAM

When dealing with pressures in OpenFOAM, it is important to be aware of the somewhat unusual unit used to express them, namely  $m^2s^{-2}$  [3]. This is the unit of the so-called “kinematic pressure”  $P$ , which is given by the pressure  $p$  and the constant mass density  $\rho_0$ , by the following relation (Wiki, n.d.):

$$P = \frac{p}{\rho_0} \quad (2.9)$$

Thus, when combining Eq. (2.3) and (2.9) to find an equation that gives us the kinematic pressure loss  $\Delta P$ , the density  $\rho$  is eliminated:

$$\Delta P = gh_f = f \frac{L V^2}{d} \quad (2.10)$$

Since the Darcy friction factor does not appear to be given directly in the OpenFOAM code, finding a relation to allow checking whether the friction factors maintain a reasonable value is useful. This is done simply by rearranging Eq. (2.10) to give the Darcy friction factor  $f$  as follows:

$$f = \Delta P \frac{d}{L V^2} \quad (2.11)$$

### 2.5.2 Estimating the parameters $k$ and $\varepsilon$ of the k- $\varepsilon$ model

In order to apply the k- $\varepsilon$  model to a specific CFD case, it is necessary to set the “inlet distributions” of  $k$  and  $\varepsilon$  for the actual case. If measurements of  $k$  and  $\varepsilon$  are not available, and relevant values are not available from literature, it is possible to obtain crude approximations for  $k$  and  $\varepsilon$  in internal flows, based on the turbulence intensity  $T_i$  and the characteristic length (or equivalent pipe radius)  $L$  of the equipment.

### Estimating the turbulent kinetic energy $k$

The turbulent kinetic energy  $k$  is then given by [5]:

$$k = \frac{3}{2}(U_{\text{ref}}T_i)^2 \quad (2.12)$$

where  $U_{\text{ref}}$  is the mean flow velocity. The turbulence intensity  $T_i$  is given by [6]:

$$T_i = I \equiv \frac{u'}{u_{\text{avg}}} = 0.16(Re_D)^{-1/8} \quad (2.13)$$

where  $u'$  is the root-mean-square of the velocity fluctuations,  $u_{\text{avg}}$  is the mean flow velocity, and  $Re_D$  is the Reynolds number.

### Estimating the turbulent dissipation rate $\varepsilon$

The turbulent dissipation rate  $\varepsilon$  is estimated by:

$$\varepsilon = C_\mu^{3/4} \frac{k^{3/2}}{l} \quad (2.14)$$

where  $C_\mu \approx 0.09$  is an empirical constant,  $k$  is the turbulent kinetic energy from (1.8), and  $l$  is the turbulence length scale.

In fully developed duct flows, calculating an approximated turbulent length scale  $l$  may be as simple as:

$$l = 0.07d \quad (2.15)$$

where  $d$  is the hydraulic diameter of the duct.

When it comes to wall-bounded flows in which the inlets involve a turbulent boundary layer, one depend on the boundary layer thickness  $\delta_{99}$  to calculate the turbulence length scale  $l$ :

$$l = 0.4\delta_{99} \quad (2.16)$$

For a turbulent boundary layer on a flat plate, the boundary layer thickness  $\delta$  is given by [2]:

$$\frac{\delta}{x} \approx \frac{0.37}{\text{Re}_x^{1.5}} \quad (2.17)$$

where  $x$  is the distance travelled along the plate in the primary flow direction.

### 3 Relevant previous work

The following chapter aims to be a summary of some of the most relevant work carried out previous to this thesis, primarily covering CFD analyses of spiral casings.

#### 3.1 “Analysis of flow in the spiral casing using a streamline upwind Petrov Galerkin method”

This paper is interesting because it analyses and displays both velocity and pressure contours from inside the spiral casing. Unfortunately it does not seem to include the stay vanes in the mesh. It has, however, successfully managed to plot the so-called Dean vortices in the tube-shaped part of the spiral casing, as well as the velocities at the outlet of the spiral casing when neglecting the stay vanes. However, since the simulation does not include the stay vanes, it might not give an accurate estimate of the flow distribution between the various channels. [7]

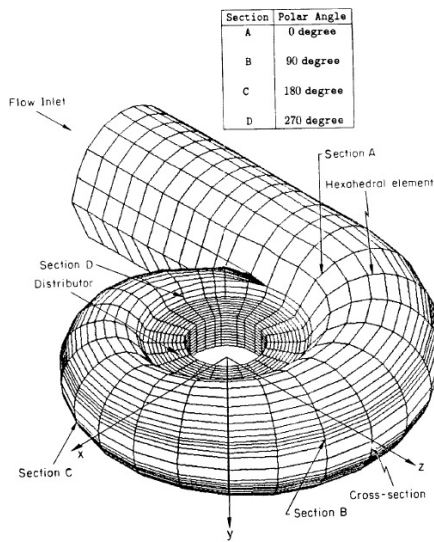


Figure 3.1.1 [7]: Mesh for the spiral casing, which appears to have been modeled without stay vanes

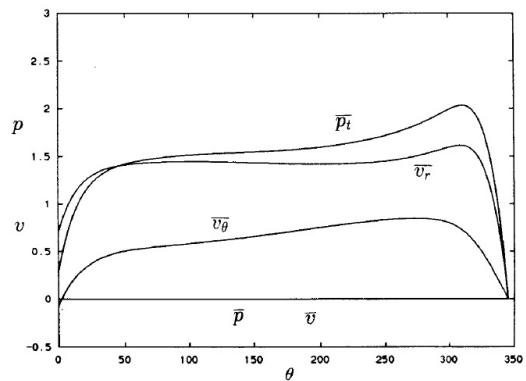


Figure 3.1.2 [7]: Average flow characteristics at the outlet of the spiral casing, as a function of the angular location (polar angle)



### 3.2 “Assessment of turbulence modelling for CFD simulations into hydroturbines: Spiral casings”

In this paper, CFX 5.5.1 was applied to simulate the flow going through a model consisting of a 90 degree bend and the spiral casing of a Kaplan turbine. An interesting aspect of this thesis is the application of three different types of turbulence models: the two-equation models  $k-\varepsilon$  and  $k-\omega$ , and a one-equation model called KE1E. In addition, an experimental investigation using Laser Doppler Velocimetry (LDV) had been carried out on a specific cross-section in the spiral casing (see Figure 3.2.3 and 3.2.4), and the experimental results were compared to the simulated results.

Unfortunately, the conduit and spiral casing geometry is more box- or cake-shaped than a typical Francis spiral casing, and the flow direction at the spiral casing outlet is vertical rather than horizontal. [8]



Figure 3.2.1 [8]: Full overview of a simulated mesh, with a 90 degree bend located in close vicinity of the cake-shaped spiral casing

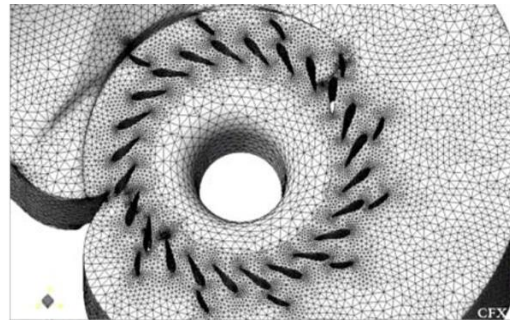


Figure 3.2.2 [8]: A close look at the mesh surrounding the stay and guide vanes, which appear as black, droplet-shaped holes in the mesh

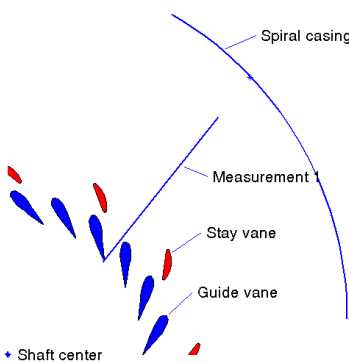


Figure 3.2.3 [8]: The location of the measured cross-section, seen from above

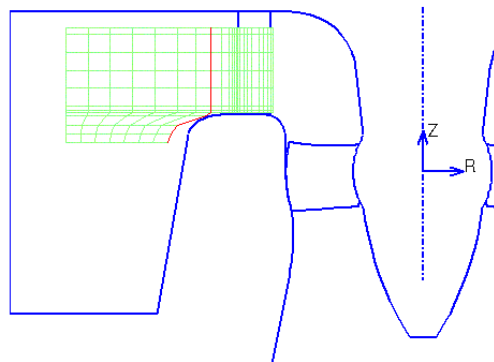


Figure 3.2.4 [8]: A vertical cross-section of the left side of the Kaplan spiral casing and runner, with the measured cross-section coloured in green

### 3.3 “Structure- and fluid-borne acoustic power sources induced by turbulent flow in 90° piping elbows”

This paper has aimed to simulate the vibro-acoustic power spectra induced to a 90 degree piping elbow. In this process, CFD has been applied to simulate a detailed flow field through the bend, and both perpendicular slices and velocity profiles have been plotted successfully. The main geometric parameters of the pipe are mean radius of curvature  $R=4.50''$  and internal pipe diameter  $d=3.50''$ , yielding a relative radius  $R/r = 2 \cdot 4.50/3.50 \approx 2.57$ . This relative radius lies between the two relative radiuses applied in Chapter 4 in this thesis, but it is interesting that the figures below show similar tendencies as those found in this thesis.

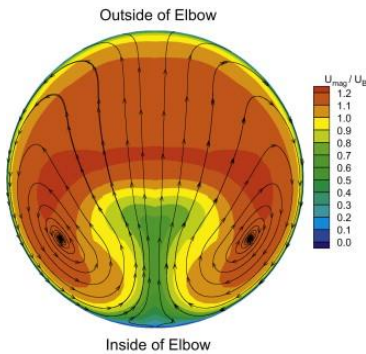


Figure 3.3.1 [9]: Slices showing secondary flow pattern at outlet of pipe bend

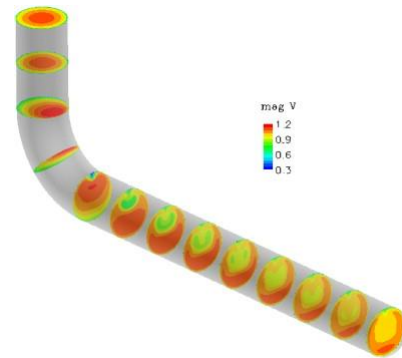


Figure 3.3.2 [9]: Slices of velocity magnitude through and downstream of a 90 degree pipe bend

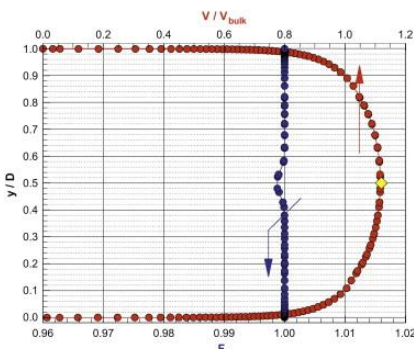


Figure 3.3.3 [9]: Velocity profile, plotted in red, in the fully develop region upstream of the pipe bend

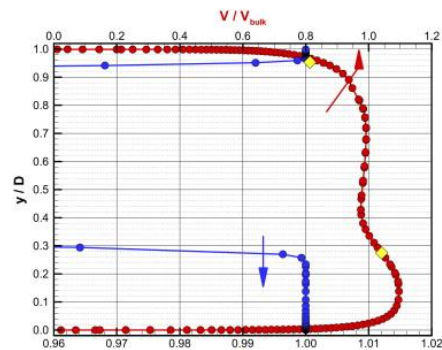


Figure 3.3.4 [9]: Velocity profile, plotted in red, near the exit of the computational domain downstream of the pipe bend.

## 4 Bend simulations using OpenFOAM

The following chapter describes simulations that were carried out in order to get an overview of the influence of various bend geometries on the downstream flow. The simulations were carried out in OpenFOAM, both because of the flexible possibilities OpenFOAM yields concerning defining your own mesh, and the author's good experience with this specific software.

### 4.1 Definition of geometries

The water conduits simulated in this chapter are determined to be shaped like two perfect cylinders, connected by a bend, which also has perfectly circular cross-sections. The parameters of the geometries described were largely chosen due to simplicity: Choosing round relative radii and bend angles makes it more likely that comparable experimental data is available, which allows to compare to the results yielded from the simulations.

Geometry	$R/r$	$\phi$
I	2	$45^\circ$
II	8	$45^\circ$
III	2	$90^\circ$
IV	8	$90^\circ$

Table 4.1 gives an overview of the difference between the geometries used for various bends. The definition of the relative radius  $R/r$  and the bend angle  $\phi$  is illustrated in Figure 2.1 in Chapter 2. Note that the angle  $\phi$  is measured as the angular distance between the bend inlet and the bend outlet, thus it will equal the angle between the centerlines of the pipes upstream and downstream of the actual bend.

Table 4.1: Parameters of simulated geometries

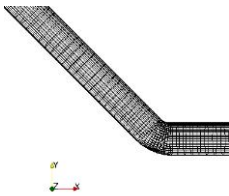


Figure 4.1.1: Geometry I

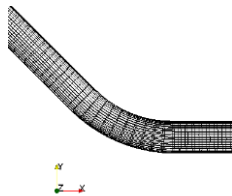


Figure 4.1.2: Geometry II

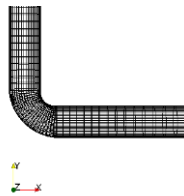


Figure 4.1.3: Geometry III

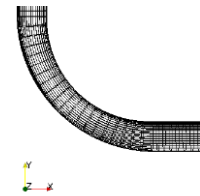


Figure 4.1.4: Geometry IV

## 4.2 Pre-processing in OpenFOAM

### 4.2.1 Defining number of cells

The meshes were made using blockMeshDict files, as described in the recipe given in Appendix A. The number of cells defined in the various parts of the mesh is defined in the section called “blocks” in the blockMeshDict file. For the actual bend geometries, the “blocks” section looks as follows:

```
blocks
(
    hex (0 1 2 3 4 5 6 7) (20 20 40) simpleGrading (1 1 1) //Downstream
    hex (4 5 6 7 8 9 10 11) (20 20 10) simpleGrading (1 1 1) //Bend
    hex (8 9 10 11 12 13 14 15) (20 20 120) simpleGrading (1 1 1) //Upstream
);
```

In each line started by “hex”, the 8 digits inside the first pair of parentheses represent 8 vertices forming the 8 corners of a hexagonal block. In order to make sure that the pipes become cylindrical and not hexagonal, the “arc vertices” in Appendix A are added.

The next pair of parentheses in each line represents the number of cells along each of the three dimensions of the blocks. The parenthesis (20 20 40) defines that the cross-section of the downstream pipe has 20x20 (a total of 400) cells, while the final number 40 defines that there are 40 cells in the axial direction of the pipe. Thus, the total number of cells for this mesh becomes:

$$20 \cdot 20(40 + 10 + 120) \text{ cells} = 68000 \text{ cells}$$

### 4.2.2 Defining boundary conditions

The location of the various patches “Inlet”, “Wall” and “Outlet”, which were used in the simulated geometries, was defined in the blockMeshDict file. Their boundary conditions, however, are defined in the various files in the /0 directory. When using a solver for turbulent flow, like “simpleFoam” for this case, it is necessary to choose a turbulence model, and for this case the simple k-ε model is chosen. This model requires the following boundary conditions to be defined: velocity  $U$ , pressure  $p$ ,

turbulent kinetic energy  $k$  and turbulent dissipation rate  $\varepsilon$ . These parameters have been defined according to Table 4.2.

<b>Parameters</b>	<b>Inlet</b>	<b>Wall</b>	<b>Outlet</b>
Velocity $U$	type fixedValue  value uniform (2.5 -2.5 0);	type fixedValue  value uniform (0 0 0);	type zeroGradient
Pressure $p$	type zeroGradient	type zeroGradient	type fixedValue  value uniform 0;
Turbulent .kinetic energy $k$	type fixedValue  value uniform 0.01107;	type kqRWallFunction  value uniform 0.01107;	type zeroGradient
Turbulent dissipation rate $\varepsilon$	type fixedValue  value uniform 0.002734;	type epsilonWallFunction  value uniform 0.002734;	type zeroGradient

*Table 4.2: Boundary conditions at the various patches*

## 4.3 Post-processing using ParaView

OpenFOAM does not have its own GUI for post-processing, so this task is usually performed using another software called ParaView. Once all the pre-processing is done and the simulation has been run, it is possible to watch the results in ParaView by writing “paraFoam” in the terminal window. When pressing “Apply” in ParaView, the model will appear. Note the time-step must be adjusted to the desired one (steady state in this case) for the desired results to appear.

### 4.3.1 Creating Slice views as used in Chapter 4.4.1

Now there should be a drop-down list available at the upper left area of the window, which in default is set to “Solid Color”, making the model grey. This drop-down list allows colouring the model according to velocity  $U$  or pressure  $p$ . However, until the model has been sliced, you will only be able to see the coloured values of these parameters at the surface of the model. To display the inside of the model, click “Filters” at the top of the window, go to “Common” and choose “Slice”. According to the way the geometry is set in the blockMeshDict of the actual simulations, the following setup must be used in the “Object Inspector” menu for the Slice:

```
Origin      [0      ][0      ][0      ]
Normal [0      ][0      ][1      ]
```

Now the Slice plots in Chapter 4.4.1 should appear.



Figure 4.3.1: There is also a Slice button available in one of the upper toolbars.

### 4.3.2 Plotting velocity profiles as used in Chapter 4.4.2

When adjusting the drop-down list described in the previous subchapter, make sure that it is set to velocity  $U$ , as the velocity is what we are aiming to plot. As also described in the previous subchapter, the drop-down list called “Filters” should be clicked (upper right corner of Figure 4.4). However, once inside Filters click “Data Analysis” and “Plot Over Line”. You will now be asked to define the start and end point (“Point 1” and “Point 2”, respectively). These coordinates will depend on the geometry you are plotting, and the which plane and position you desire to get your plot from. Once the correct start and end point is chosen, click “Apply”. In default mode, “U (Magnitude)” and “p” will usually be plotted automatically.

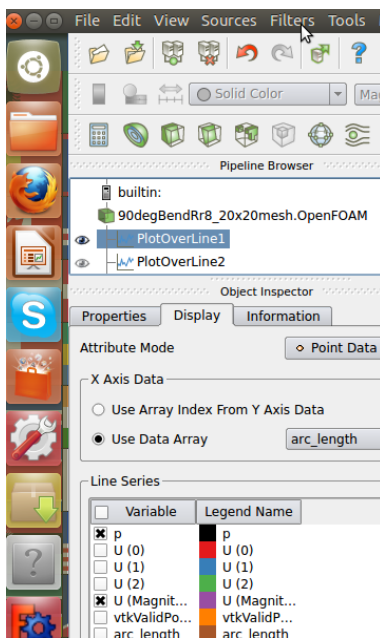


Figure 4.3.2: Locations of the drop-down lists “Filters” and “Solid Color”, the tabs “Properties” and “Display”, and the variables “p” and “U (Magnitude)”

When defining start and end point, you are located in the “Properties” tab of the Object Inspector. In order to choose which variables to plot, the colour of the plots, and their tags, click the “Display” tab in the Object Inspector. Since all the pipe geometries described in this report are parallel to the x axis after the outlet of the bend, the variable with the default name “U (0)” was chosen for plotting. By double clicking at the desired variable in the “Legend Name”, you may choose its colour. By left clicking at the area where the legend name is written, you may rename the variable. Plotting velocity profiles similar of those in Chapter 4.4.2 should now be possible.

## 4.4 Results from bend simulations

### 4.4.1 Pressure and velocity fields in bends

All of the following figures are taken from the symmetry plane of each mesh, which were 3D bend models. The simulations were carried out using the  $k-\varepsilon$  model, and the results look reasonable compared to similar simulations.

#### 4.4.1.1 45 degree bend with relative radius $R/r=2$

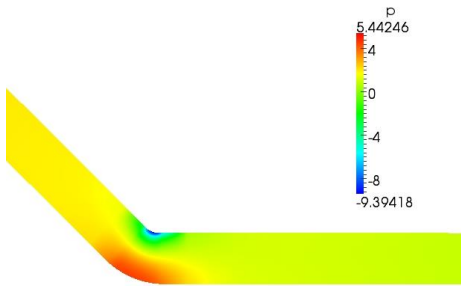


Figure 4.4.1.1a: Pressure field

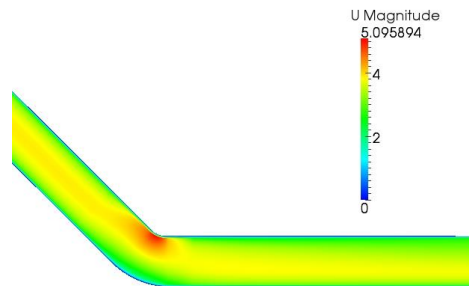


Figure 4.4.1.1b: Velocity field

#### 4.4.1.2 45 degree bend with relative radius $R/r=8$

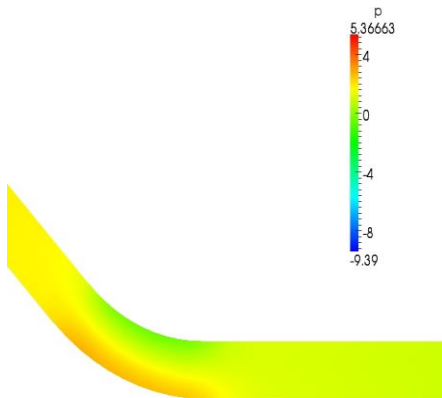


Figure 4.4.1.2a: Pressure field



Figure 4.4.1.2b: Velocity field



### 4.4.1.3 90 degree bend with relative radius $R/r=2$

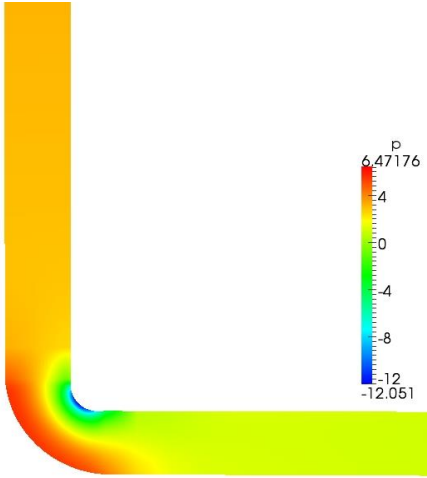


Figure 4.4.1.3a: Pressure field

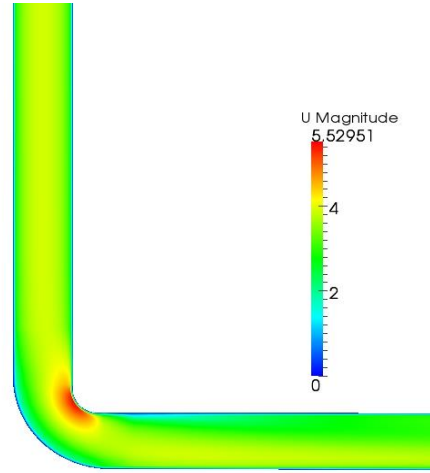


Figure 4.4.1.3b: Velocity field

### 4.4.1.4 90 degree bend with relative radius $R/r=8$

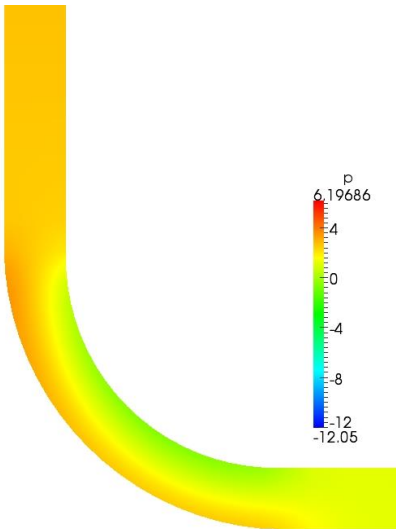


Figure 4.4.1.4a: Pressure field

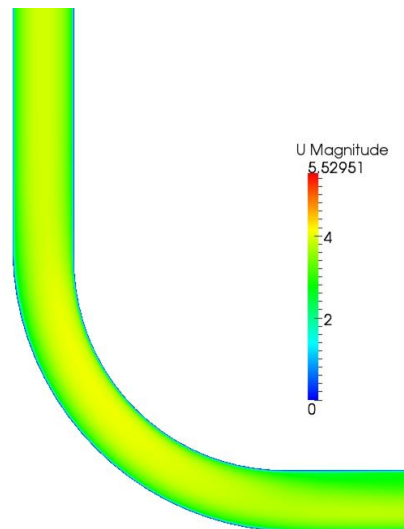


Figure 4.4.1.4b: Velocity field

## 4.4.2 Axial velocity profiles downstream of various bend geometries

The following two pages display velocity profiles downstream of bends with the same geometries as those displayed in the previous two pages. The location of Plane AA and Plane BB is the same as that given in Chapter 2.3. Along the abscissa, the values 0 and 1 represent the inside and outside of the bend, respectively. Along the ordinate is the velocity [m/s], and the average velocity along the entire pipe cross-section is 3.5355 m/s in each simulation.

The various colours of the plots represent various axial distances from the outlet of the bends, for which the velocity profiles are plotted. The axial distance from the outlet of each bend is symbolized by  $x$ , while for each simulation, the diameter  $D = 1\text{ m}$ . These parameters allow forming the dimensionless parameter  $x/D$ .

Once well-developed, the velocity profiles seem to show similar characteristics as the plots from previous work and experiments displayed in Figure 2.2.

### 4.4.2.1 45 degree bend with relative radius $R/r=2$

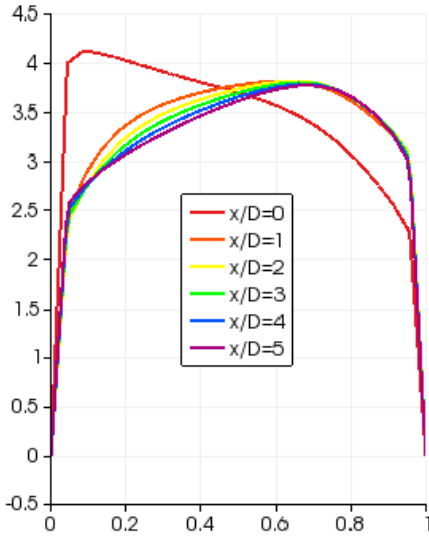


Figure 4.4.2.1a: Plane AA

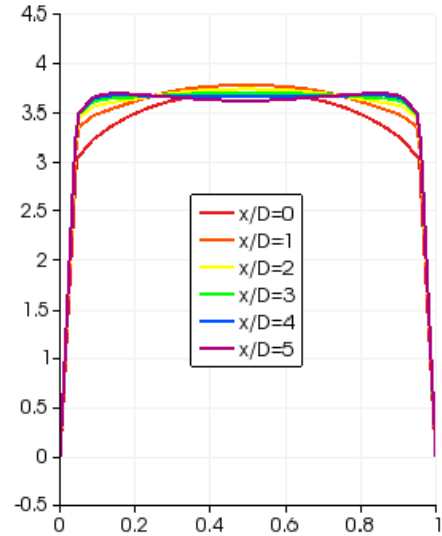


Figure 4.4.2.1b: Plane BB

### 4.4.2.2 45 degree bend with relative radius $R/r=8$

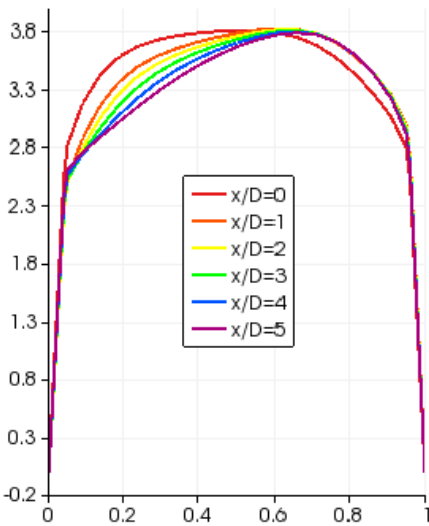


Figure 4.4.2.2a: Plane AA

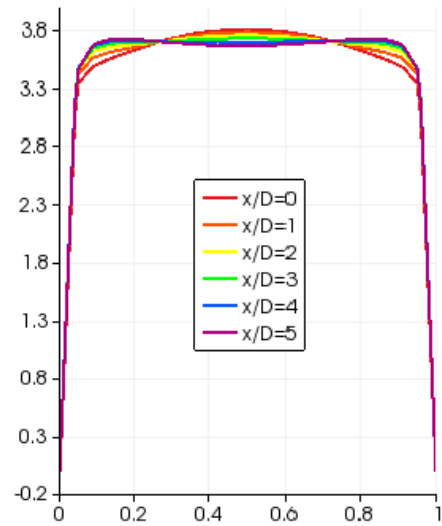


Figure 4.4.2.2b: Plane BB

### 4.4.2.3 90 degree bend with relative radius $R/r=2$

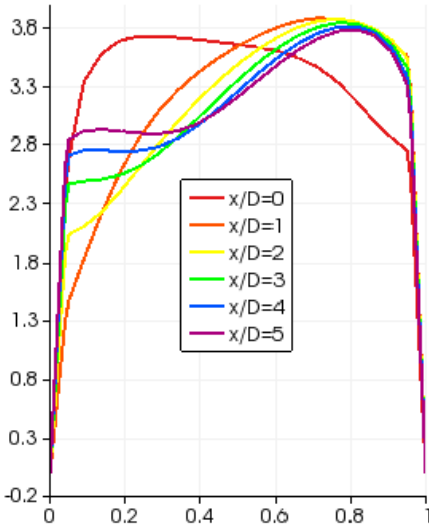


Figure 4.4.2.3a: Plane AA

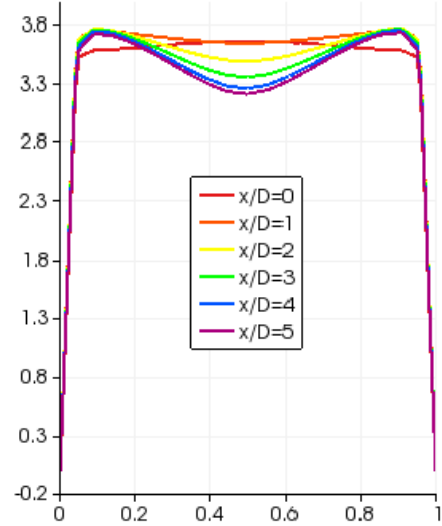


Figure 4.4.2.3b: Plane BB

### 4.4.2.4 90 degree bend with relative radius $R/r=8$

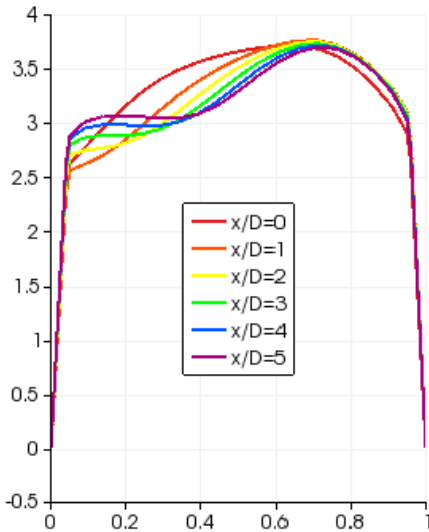


Figure 4.4.2.4a: Plane AA

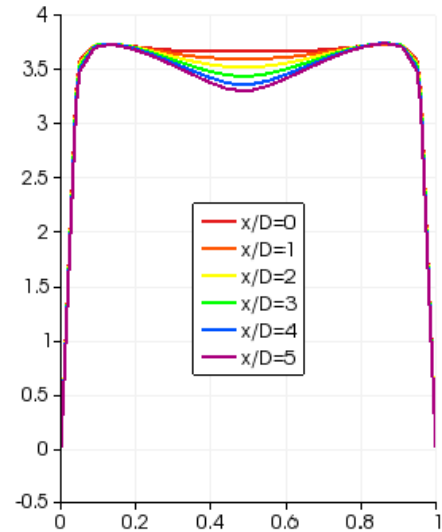


Figure 4.4.2.4b: Plane BB

### 4.4.3 Axial velocity components plotted against axial distance downstream of various bend geometries

Similarly as for the plots in chapter 4.4.2, the axial velocity  $u$  is plotted along the ordinate in the following subchapter, and the average velocity over the full pipe cross-section is 3.5355 m/s. However, for the following plots the dimensionless axial distance  $x/D$  downstream of the bend outlet is plotted along the abscissa, covering the range  $0 \leq x/D \leq 20$  for the 45 degree bends and  $0 \leq x/D \leq 10$  for the 90 degree bends.

The locations of the five velocity components plotted on the following two pages are defined in Figure 4.4.3.

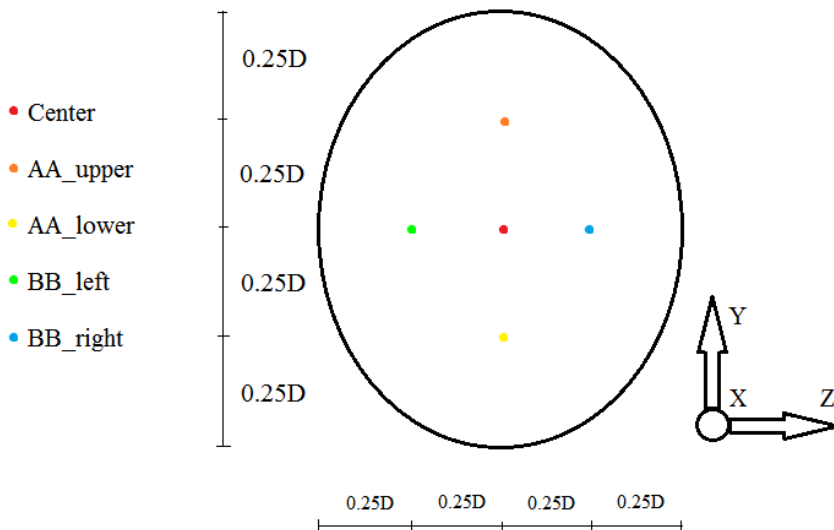


Figure 4.4.3: The location of the various velocity components plotted on the following two pages, defined in the YZ plane, relative to the pipe walls

#### 4.4.3.1 45 degree bend with relative radius $R/r=2$

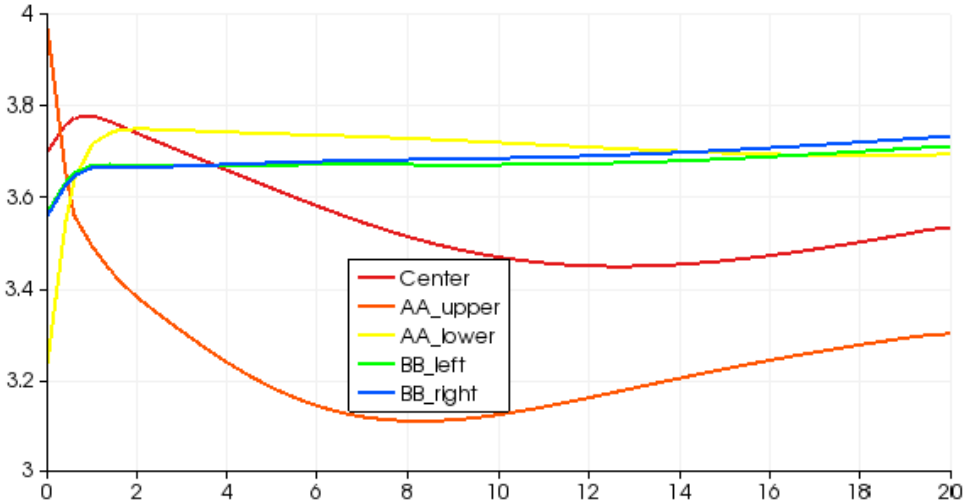


Figure 4.4.3.1: When dealing with a 45 degree bend with  $R/r=2$ , the convective acceleration  $\frac{\delta u}{\delta x} = 0$  at  $x/D \approx 12.6$  for the “Center” velocity component.

#### 4.4.3.2 45 degree bend with relative radius $R/r=8$

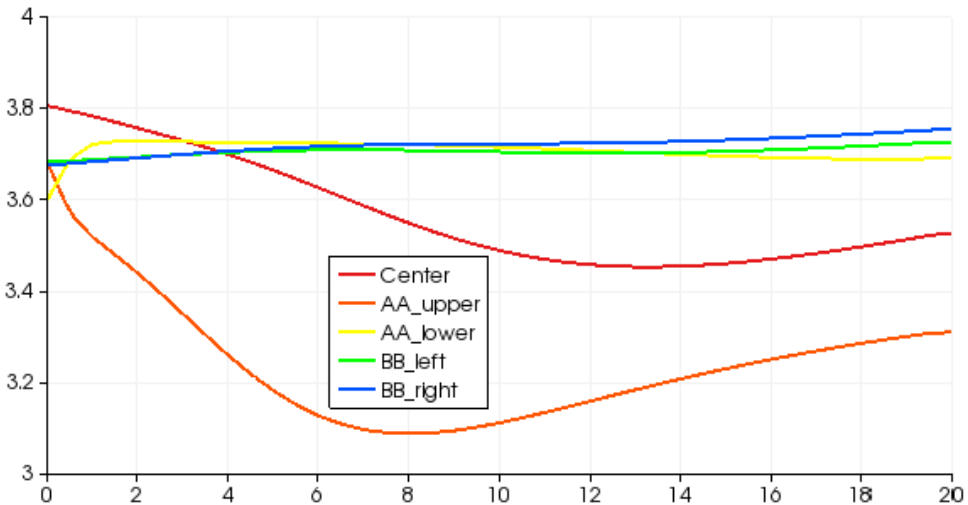


Figure 4.4.3.2: When dealing with a 45 degree bend with  $R/r=8$ , the convective acceleration  $\frac{\delta u}{\delta x} = 0$  at  $x/D \approx 13.4$  for the “Center” velocity component.

### 4.4.3.3 90 degree bend with relative radius $R/r=2$

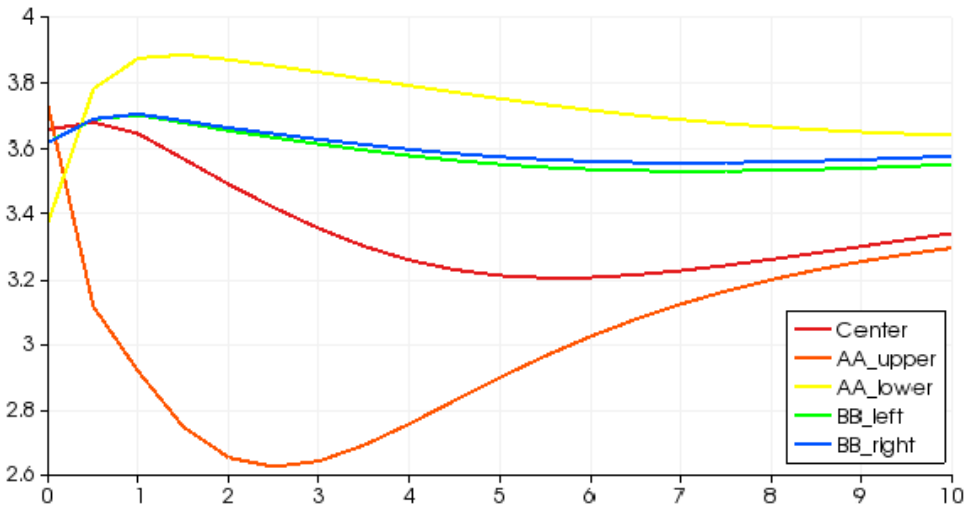


Figure 4.4.3.3: When dealing with a 90 degree bend with  $R/r=2$ , the convective acceleration  $\frac{\delta u}{\delta x} = 0$  at  $x/D \approx 5.5$  for the “Center” velocity component.

### 4.4.3.4 90 degree bend with relative radius $R/r=8$

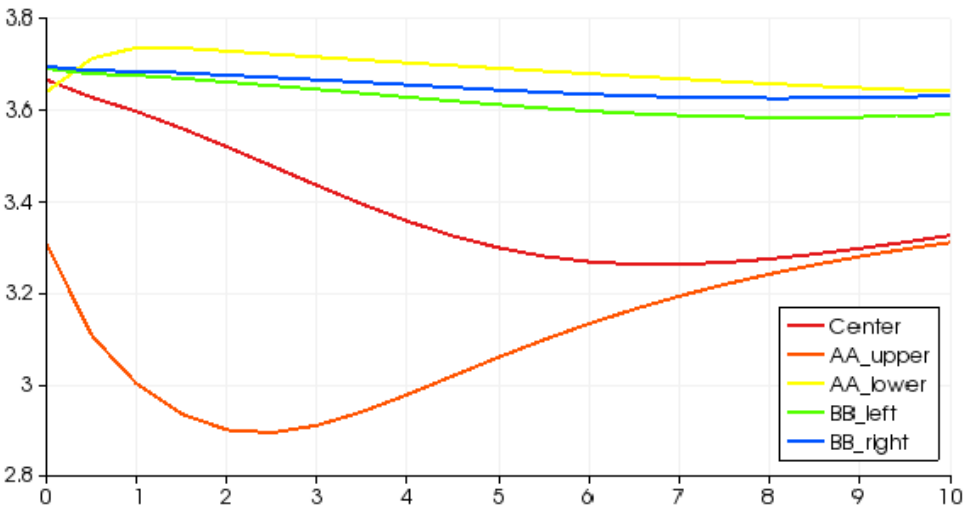


Figure 4.4.3.4: When dealing with a 90 degree bend with  $R/r=8$ , the convective acceleration  $\frac{\delta u}{\delta x} = 0$  at  $x/D \approx 7.0$  for the “Center” velocity component.

## 5 Spiral casing simulations using CFX

The following chapter describes simulations that were carried out in order to get an overview of the ability of NTNU's Tokke spiral casing to distribute the inlet flow into the turbine equally from all sides. The simulations were carried out using ANSYS CFX, due to difficulties with importing CAD files into OpenFOAM, and the status of ANSYS as a well-established and validated simulation software.

### 5.1 Definition and preparation of geometry

A CAD model of the Tokke spiral casing model, which is currently installed at the Hydropower Laboratory at NTNU, has already been drawn in Pro/Engineer, and saved as a ".prt" file. This formed the basis for the spiral casing simulations carried out in this report. Initially, the CAD model was drawn to represent the solid parts of the spiral casing, but the model was edited to represent the internal flow volume, by PhD Bjørn Winther Solemslie. Once the geometry was successfully drawn, it was exported as a STEP file, in order to allow it to be imported into ANSYS for meshing.

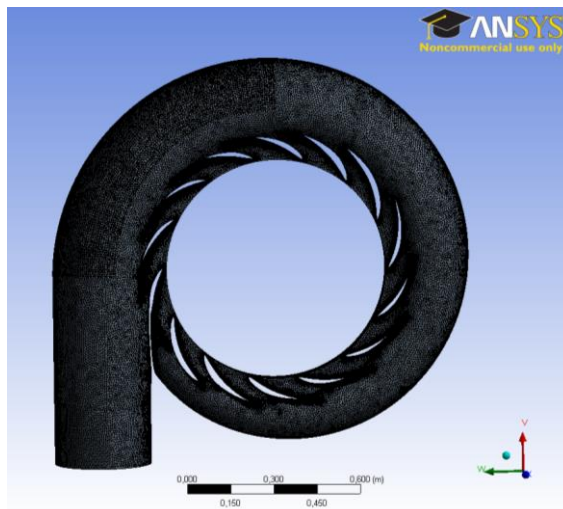


Figure 5.1: The internal flow volume of the Tokke spiral casing model, meshed in ANSYS



## 5.2 Pre-processing in ANSYS

The navigation between the various parts of the processing in ANSYS is done in ANSYS Workbench. Once inside the Workbench, click “Import”, choose “Geometry file” in the drop-down list, and select the desired STEP file. If successful, you will get a green checkmark next to “Geometry” in your Project Schematic.

### 5.2.1 Meshing in ANSYS

In order to get to the Meshing software, go to “Analysis Systems” in your Toolbox and double-click at “Fluid Flow (CFX)”. You will now get another schematic component named “Fluid Flow (CFX)” in your Project Schematic, next to the one called “Geometry”. Each of these schematic components will have a cell named “Geometry”. In order to give the Geometry cell of the CFX schematic component a green checkmark, drag the Geometry cell from the Geometry component, and drop it in the Geometry cell of the CFX component. If successful, both of the cells will be checked green, and linked by a blue line.

In your CFX component, there should be a cell called “Mesh”, which should be marked by a lightning bolt. Double-click in this cell, and a window called “Meshing” will be opened. If all settings are left at default, and the “Generate Mesh” button is pushed, the software will generate a mesh with 5 127 891 elements for the Tokke spiral casing model. The large number of elements is largely caused by the high concentration of small elements in the curvature around the stay vanes. Your “Mesh” cell in the Project schematic should now have a green checkmark.

### 5.2.2 Defining boundary conditions in CFX

The next step in the CFX component is the Setup cell. When double-clicking it, you will get into CFX-Pre. Once the CFX-Pre window is open, click “Insert” followed by “Boundary”, and give a name to the surface whose boundary condition you are about to specify.

For the Inlet boundary, the “Boundary Type” should naturally be “Inlet”. The area may be specified simply by clicking at the desired surface, which should give the borders between the elements located in the inlet surface a green colour. Once “Location” is set correctly in the “Basic Settings” tab, go to the

“Boundary Details” tab, and set “Normal Speed” to  $2.8645\text{ m/s}$ . This speed corresponds to a volumetric flow  $Q = 0.250\text{ m}^3/\text{s}$ , when the inlet cross-section has a diameter  $d = 0.33335\text{ m}$ . When finished, remember to click “Apply”, before “Ok”.

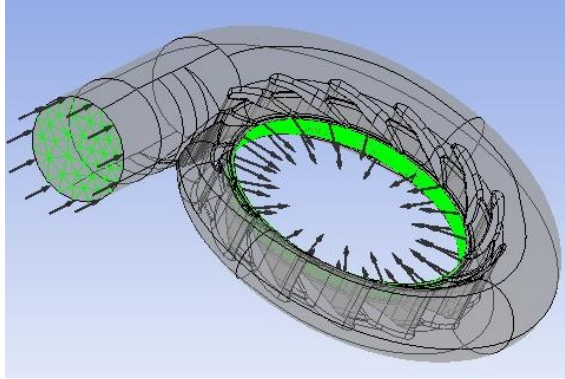


Figure 5.2: What the model should look like in CFX-Pre after defining Inlet and Outlet boundaries.

When defining the Outlet boundary, note that the mesh might have the outlet area divided into two parts. To specify both surfaces as outlet areas, hold Ctrl when selecting the second surface. For simplicity, set “Relative Pressure” to 0 in the Boundary Details tab.

Once you have defined the Inlet and Outlet boundaries, you may define the remaining boundaries simply by editing the boundary called “Default Domain Default”. The wall boundary of the spiral casing should have the Boundary Type “Wall”. Now click Apply. You may rename the Default Domain to something reasonable, like “Walls”.

When all your boundaries are defined, the Setup cell in your Project Schematic should have a green checkmark. The simulation may be started by double-clicking the “Solution” cell.

## 5.3 Post-processing in CFX

Once the simulation is finished, the post-processing may be started by double-clicking the “Results” cell. A window called “Fluid Flow (CFX) – CFD-Post” will open. In default view, the geometries in the “3D Viewer” will be limited to the borders between the boundaries defined during the pre-processing.

### 5.3.1 Colour plot of the flow field inside the spiral casing

To visualize the resulting flow field, click the drop-down list “Insert”, and choose “Volume Rendering”. Choose a name, choose whether you want to visualize the variable “Pressure” or “Velocity”, and click Apply. Now you will only be able to see the outer surface of the flow volume. Since we are interested in studying how the flow develops inside the flow volume, we will clip the spiral casing in half. This is done by clicking Insert and “Clip Plane”. First choose a name, then for “Method”, choose “XY Plane”, and set the location “Z” to 0.0 [m]. When clicking Apply, something similar to Figure 5.3 should appear:

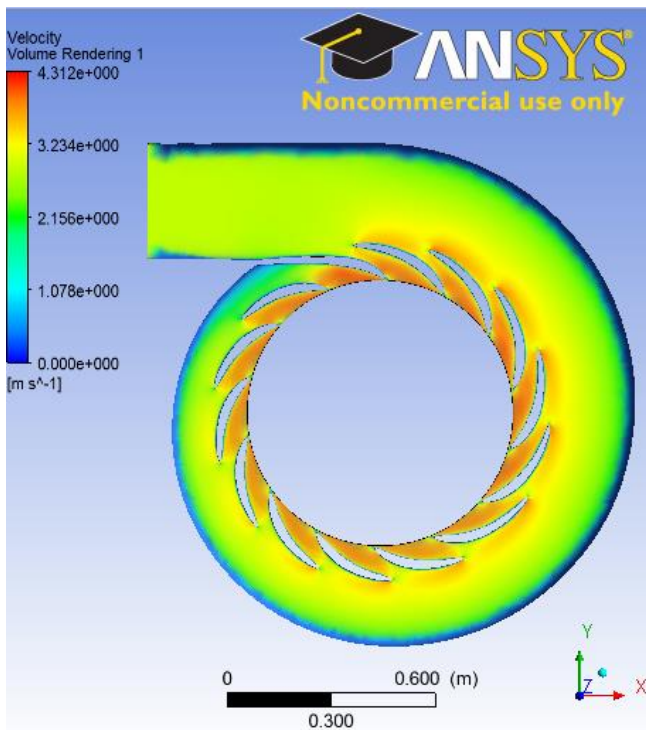


Figure 5.3:  
This figure should show up after applying “Volume Rendering” for Velocity and using a “Clip Plane” in CFX-Post.

### 5.3.2 Radial velocity plotted along the outlet of the spiral casing

In order to plot the radial velocity given by the angular location at the outlet of the spiral casing, there is a number of input parameters to be defined:

- The line one desires to plot the actual variables along, for which “Polyline” is a good solution.
- The variable representing the angular location (referred to as “Angle”), which describes where the various radial velocities are located, as well as allowing to calculate these.
- The variable representing the radial velocities flowing towards the runner.
- The setup of the chart plotting the angular location vs. radial velocity.

#### Defining the Polyline

Go to Insert → Location → Polyline, and make the following selections:

Method:                    Boundary Intersection  
 Boundary List :        Outlet  
 Intersect With: Outlet

Now press Apply.

#### Defining the angular location “Angle”

For creating the variable “Angle”, first go to the tab “Expressions”, and click Insert → “Expression” to insert a new expression. This may be named “ExpAngle”. In the “Definition” tab of the expression, write :

```
atan2 (X, Y)
```

In this way, “Angle” will be defined as zero at the inlet of the spiral casing. Press Apply. Now go to the “Variables” tab, and click Insert → Variable, and name the variable “Angle”. At the “Expression” drop-down list, choose “ExpAngle”, and press Apply.

#### Defining the radial velocities

Insert another expression in the Expressions tab, and name it “ExpRadialvelocity”. In the “Definition” tab of the expression, write:

```
-Velocity u*sin (Angle)-Velocity v*cos (Angle)
```

Now insert a variable named “Radial velocity”, and link it to the expression “ExpRadialvelocity”. Press Apply.

**Defining the chart for plotting**

Click Insert → Chart, and the “General” tab, define “Type” as “XY”. Go to the “Data Series” tab, define a new data series, and define “Location” as your desired polyline. In the “X Axis” and “Y Axis” tabs, the variables should be defined as “Angle” and “Radial velocity”, respectively. After pressing Apply, and switching to the “Chart Viewer” tab on the right side of the window, the chart showing “Radial velocity” plotted against “Angle” should appear.

## 5.4 Results from spiral casing simulations

In the following subchapter, the main results from the CFD simulations of the Tokke spiral casing model, carried out in ANSYS CFX, are being presented. In order to validate the mesh independency, the simulations have been carried out using two different meshes with different number of cells: one with 1 641 075 and the other with 5 127 891 cells. The results for both of these meshes will be presented in the following.

The pressure and velocity fields are plotted in what is referred to as the “centered” horizontal plane, emphasizing that the slice applied for plotting is located in the very middle of the vertical axis of the model, which for this model corresponds to the plane  $Z=0$ .

### 5.4.1 Velocity fields in horizontal plane

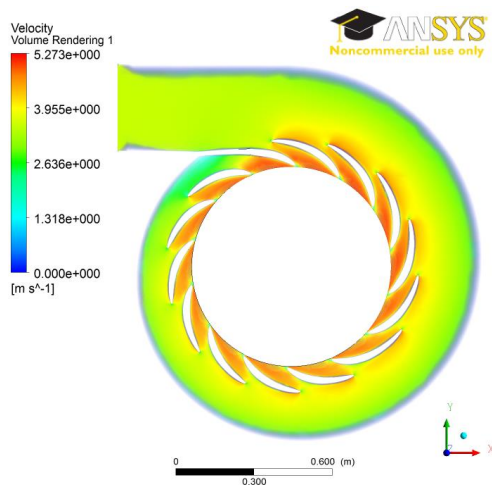


Figure 5.4.1a: 1 641 075-cell mesh

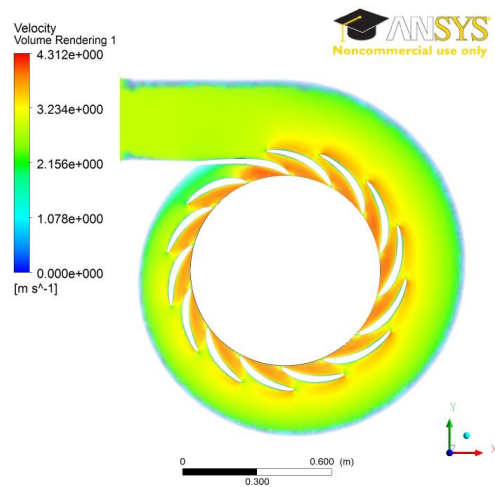


Figure 5.4.1b: 5 127 891-cell mesh

## 5.4.2 Pressure fields in horizontal plane

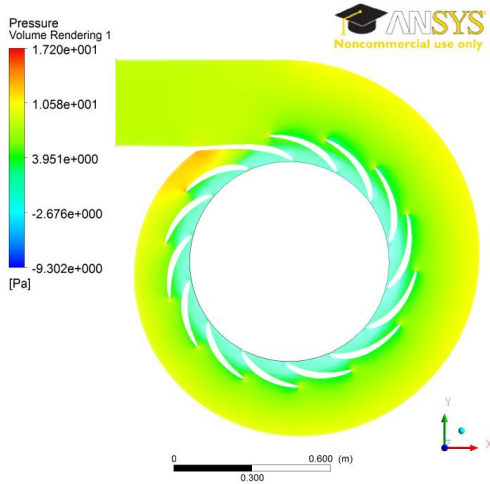


Figure 5.4.2a: 1 641 075-cell mesh

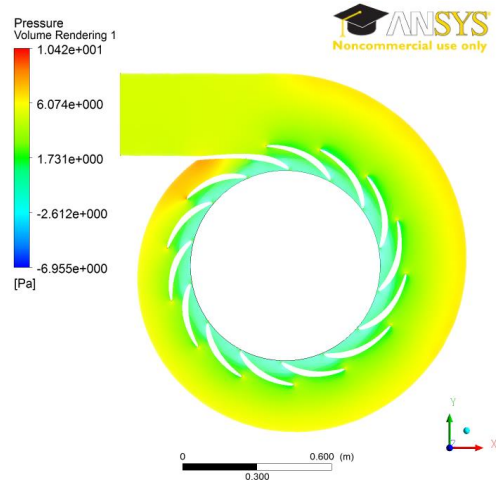


Figure 5.4.2b: 5 127 891-cell mesh

## 5.4.3 Streamlines below horizontal plane, with spiral casing surface

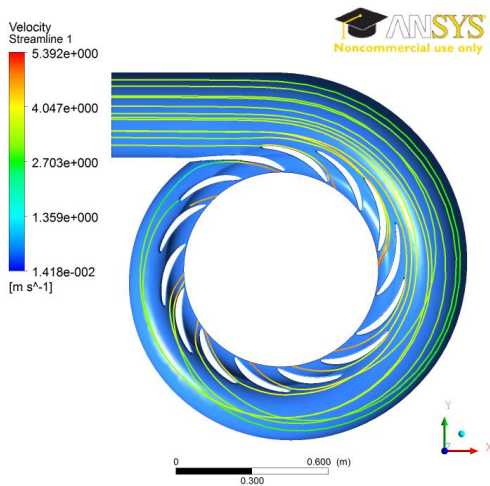


Figure 5.4.3a: 1 641 075-cell mesh

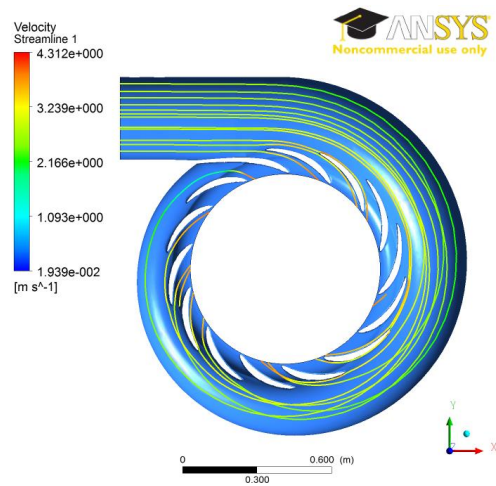


Figure 5.4.3b: 5 127 891-cell mesh

### 5.4.3 Radial velocity at the outlet of the spiral casing

Based on the problem description this thesis is based on, one of the most interesting outputs from the CFD simulations of the spiral casing is the velocity distribution at the outlet. It was resonated in Chapter 2.4 that an even velocity distribution with flow velocities close to the ideal flow velocity is likely to be beneficial for the hydraulic efficiency of the turbine.

#### 5.4.3.1 Definition of angular location at spiral casing outlet

In the figures on the following pages, the radial velocity is plotted against what is referred to as the “angular location” or “Angle”. This parameter is defined in the figure below, denoted as  $\alpha$ .

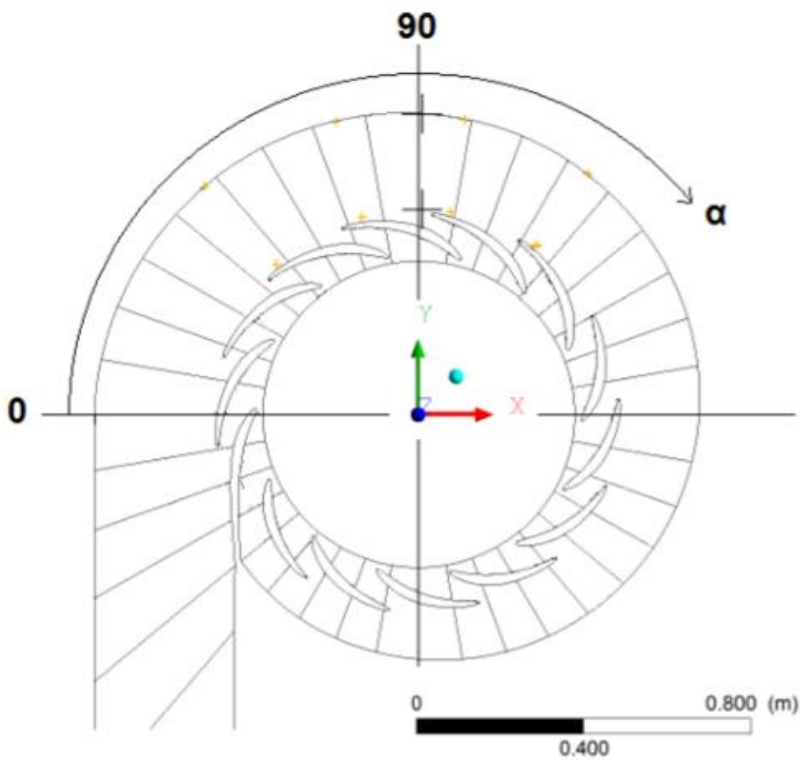


Figure 5.4.3.1: The definition of the angular location, which is being referred to on the following pages



### 5.4.3.2 Radial outlet velocity plotted against angular location

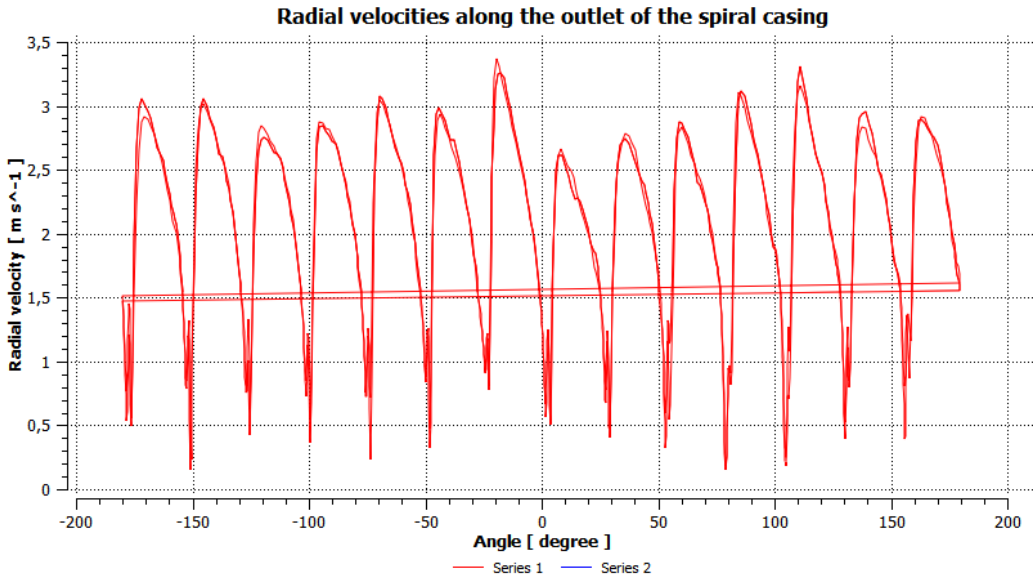


Figure 5.4.3.2a: Resulting radial velocities from a simulation with a 1 641 075-cell mesh and an inlet velocity of 3.5355 m/s

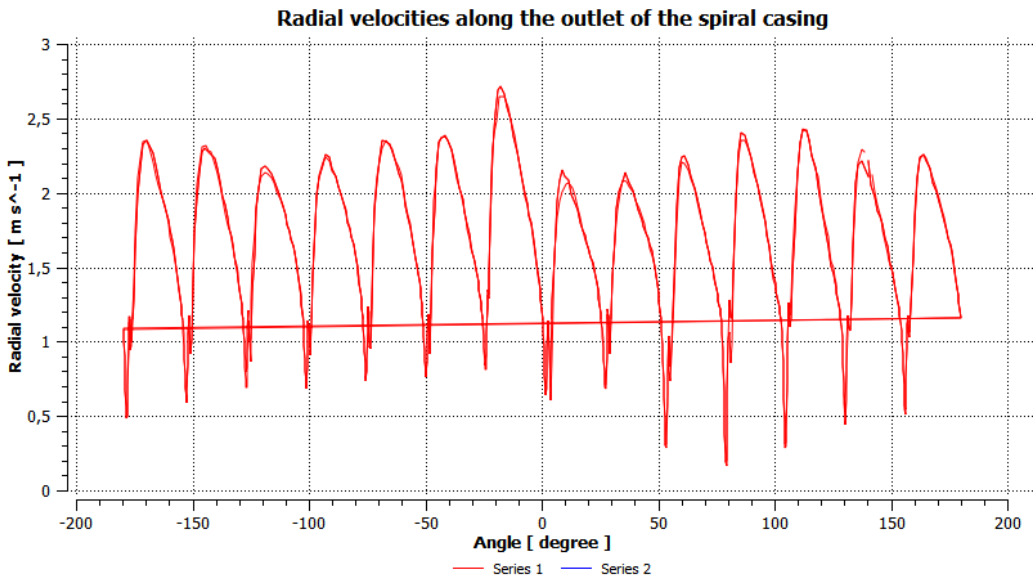


Figure 5.4.3.2b: Resulting radial velocities from a simulation with a 5 127 891-cell mesh and an inlet velocity of 2.8645 m/s



## 6 Discussion

### 6.1 Possible consequences of skewness and secondary flows at the spiral casing inlet

In Chapter 2.4, the effect of a poor distribution of flow into the runner was briefly described. References were made to literature stating that spiral casing should be designed such that the velocity field into the stay vanes, and thus the runner, becomes uniform. In chapter 4.4.2, it was shown that especially sharp-angled bends tend to cause sharply skewed velocity profiles with peak velocity skewed towards the side corresponding to the outside of the bend in Plane AA, and a secondary on each side of the pipe in Plane BB.

Since the spiral casing of a vertical axis Francis turbine is approximately symmetrical across its horizontal plane, it seems reasonable to assume that the formation of asymmetrical velocity profiles along Plane AA (as defined in Chapter 2.3) in the conduit entering the spiral casing, may lead to asymmetrical velocity fields across the horizontal plane throughout the spiral casing.

It also seems reasonable to assume that the occurrence of two secondary flows in Plane BB may lead to poor velocity distribution at the runner inlet. Since the streamlines on each side of Plane BB in the inlet conduit tend to enter the some of the first and some of the last stay vane channels, respectively, one may expect to see increased flow velocities in these specific channels when dealing with skewed inlet profiles in Plane BB.

### 6.2 Reasons for simulating penstock and bend geometries isolated from spiral casing

In this thesis, Chapter 4 was devoted to simulating various bend geometries along with straight penstocks, isolated from the spiral casing. This may seem like unnecessary efforts, when an important goal of the thesis is understanding how the bends influence the flow conditions in the spiral casing itself. However, there are two main, interconnected reasons why running simulations on penstocks and bends isolated is useful:

### **1. Getting an overview of the various flow conditions that may occur as a result of various bend geometries**

In the previous subchapter, it was argued that skewed flow conditions into the spiral casing may lead to skewed flow conditions out of the spiral casing. Based on this assumption, the knowledge of which extent various bend geometries affect the downstream flow conditions may become of great interest when choosing the conduit bend geometry of various power plants.

### **2. Significantly reduced simulation run time for lower numbers of cells**

The relationship between run time and number of cells for a specific CFD case is sometimes challenging to predict, because it depends heavily on the implementation of the solution algorithm. However, according to the author's experience, the run time may, in some cases, increase proportionally with the number of cells *squared*. I.e., doubling the number of cells yields four times longer run time. In such cases, limiting the number of cells is of great interest. Since a typical spiral casing with stay vanes is a far more complicated geometry than a penstock with a bend, isolating the penstock will reduce the run time significantly, and is especially interesting when it is desired to investigate a larger number of possible penstock geometries.

### **3. The possibility of applying outlet boundary conditions from an upstream simulation as inlet boundary conditions on a downstream simulation**

A common approach for simulating complex objects in CFD is dividing the object into smaller, less complex objects, and run the simulations separately. This may be applied on a penstock-spiral casing simulation by estimating the outlet flow field from a steady-state penstock simulation, and apply this on the inlet of a steady-state spiral casing simulation.

Although there are several arguments for breaking large simulations into smaller ones, running large complete simulations of systems like a penstock-spiral casing case may be more accurate in some cases, especially in transient phenomena are of interest. Therefore, running complete penstock-spiral casing simulations is recommended for further work on the topic described in this thesis.

# 7 Conclusions

In this chapter, the main findings during the work with this thesis are presented.

## 7.1 Undesirable effects of poor velocity distribution at the inlet of a runner

In Chapter 2.4, the basic velocity components at the inlet of a runner were presented, and it was reasoned that the magnitude of the ideal flow velocity at the inlet of the runner is given by the runner design and the rotational speed of the runner. Thus, an uneven velocity distribution at the inlet of the runner will always differ from the ideal velocity distribution, where the absolute flow velocity  $c$  equals the ideal flow velocity  $*c$  at all inlet locations.

When the flow velocity at the inlet of the runner differs from its ideal value, the flow velocity relative to the runner will not enter the runner parallel to the runner blades, which is what they would in an ideal case. Instead you will have parts of the flow field impinging on the runner blade, causing secondary flows to accelerate along the channel surface. Large formations of secondary flow are not ideal for the hydraulic efficiency of the turbine, as they complicate the pressure field in the runner channel, and cause increased friction losses.

## 7.2 The influence of bends on flow conditions

The most significant findings from the simulations carried out on bends in this thesis, using OpenFOAM, were presented in Chapter 4.4. One of the most obvious effects of applying a small relative radius ( $R/r=2$  in this case) is the tendency of the velocity profiles in Plane AA to become skewed towards the inner side of the bend, before shifting and bending towards the outer side relative to the bend. (The inner and outer side relative to the bends correspond the left and right side, respectively, of the Plane AA plots in chapter 4.4.2.) This changed location of the peak velocity occurs over a distance of  $x/D \leq 0.5$  for all small relative radius simulations carried out in this thesis. This involves sharp convective velocity gradients,  $\frac{\delta u}{\delta x}$ , and suggests that the flows occurring after bends of small relative radiuses are more chaotic than those occurring after bends of larger relative radius.

When comparing bends with a sharp angle ( $90^\circ$  in this case) to bends with a smaller angle ( $45^\circ$ ), the sharp angle bend tends to result in sharper convective velocity gradients in both Plane AA and Plane BB. Interestingly, the  $90^\circ$  degree bends develop velocity profiles that become skewed to such an extent that they develop two inflection points, even in Plane AA. The inflection point in the velocity profiles involve  $\frac{\partial^2 u}{\partial y} = 0$ , where the parameter  $y$  is located along the abscissas of the Plane AA plots in Chapter 4.4.2.

In Plane BB after all of the bends simulated, a local minimum velocity tends to occur in the middle of each velocity profile, while a local maximum occurs on each side of the velocity profile. This might be compared to having two secondary flows going through the flow side by side, and the phenomenon clearly creates the largest secondary flows after the bends with sharp angles ( $90^\circ$ ). It might be speculated whether these secondary flows might contribute to poor flow distribution at the outlet of the spiral casing.

## 8 Further work

### 8.1 Validation of the Tokke spiral casing model simulations

Validation is essential when determining whether specific CFD simulations are yielding an accurate picture of the flow phenomena in the case that is desired to investigate. According to NASA, validation is defined as “the process of determining the degree of which a model is an accurate representation of the real world from the perspective of the intended use of the model”. [15]

Considering that the Tokke spiral casing model is available in the Hydropower Laboratory at NTNU, along with some instruments for velocity and pressure measurements, there seems to be great opportunities available for verifying the results from this thesis, and from other simulations related to the topic. Indeed, during spring 2013, while this thesis was written, another thesis called “Pressure pulsations and stress in a high head Francis model turbine” (written by Julie Mari Hovland) involved carrying out pressure measurements at three locations in the “vaneless space”, located between the guide vanes and the runner. (see Figure 8.1). It is important to note that steady-state CFD simulations, carried out without a runner, naturally do not simulate pressure pulsations, but experimental data on relative static pressure may be comparable.

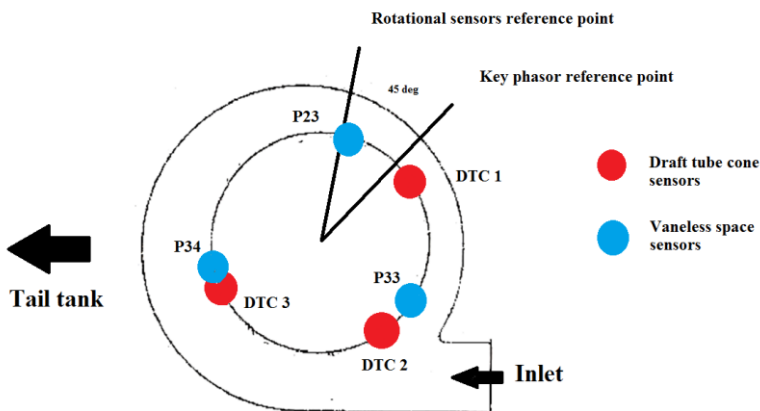


Figure 8.1 [12]: Location of pressure sensors during measurements carried out by Julie Marie Hovland and Ingeborg Lassen Bue during the spring of 2013.

As the main focus of this thesis has been the velocity field, an interesting question is

whether the openings and setup shown in Figure 8.1 may in any way be applied for carrying out velocity measurements. The author does not have sufficient insight into the setup to determine whether this is feasible, but will still present two possible velocity measurement methods, with pros and cons of each method:

### Pitot tubes

Pitot tubes are indeed available at the NTNU Hydropower Laboratory, and is based on simply measuring the difference between the stagnation pressure and the static pressure in the flow. A drawback is that it is not particularly suited for measuring fluctuating phenomena in the flow.

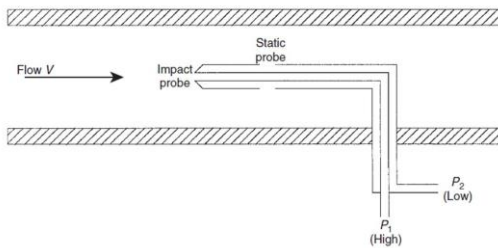


Figure 8.1.1 [17]: Setup of a basic Pitot tube used for velocity measurements.

### Hot wire/hot film anemometers

The advantage of applying a hot-wire/hot-film anemometers for flow measurement is their ability to register flow fluctuations. To the author's knowledge, hot-wire anemometers for airflow have been used recently (2013) at the NTNU Fluids Engineering Building, e.g. during these supervised by Professor Lars Roar Sætran. The drawback is that hot-wire anemometers applied on airflow are very thin and fragile, and it is likely that these are not applicable on water flow. However, hot-film anemometers should be applicable to liquids.

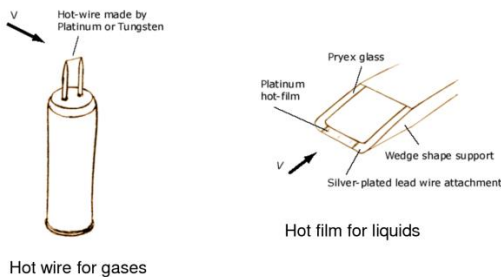


Figure 8.1.2 [18]: Setup of a basic Pitot tube used for velocity

For more information about Pitot tubes and hot-wire anemometers, the author can recommend the compendium “Hydraulisk måleteknikk” by Arne Kjølle [13].



## 8.2 Running complete penstock-spiral casing simulations

In Chapter 6.2, it was suggested to apply “outlet boundary conditions from an upstream simulation as inlet boundary conditions on a downstream simulation”. This would allow running the spiral casing at a wide range of possible inlet conditions, which should be defined according to possible penstock designs of interest. However, the author has yet to discover a satisfying method for defining complex inlet conditions in ANSYS. In a previous thesis written by Klemetsen [14], an elegant method for defining symmetrical inlet profiles using polynomial functions is described. However, converting skewed, asymmetrical 3D velocity fields to polynomial functions seems to be a rather tricky process.

Thus, the author would recommend future researchers to look into the possibility of defining the inlet field using a matrix to define the velocity field. The author can confirm that this option is possible using less developed CFD software like OpenFOAM, and this is a good reason to believe that the same option should be available using well-developed software like ANSYS.

## 8.3 The influence of valve geometries on spiral casing flow conditions

During the work with this thesis, the possibility of investigating the influence of various valves on the velocity field running into the spiral casing was suggested by Professor Torbjørn Nielsen. [16] Some interesting geometries to investigate further could be butterfly valves or spherical valves (see Figure 8.3.1 and 8.3.2).

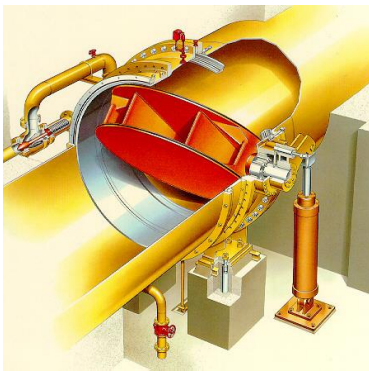


Figure 8.3.1 [19]: Butterfly valve

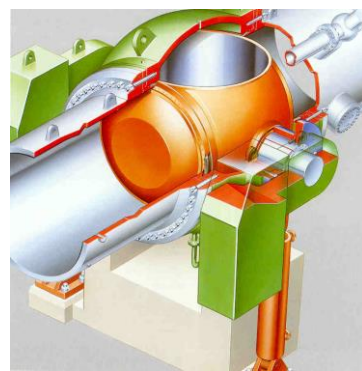


Figure 8.3.1 [19]: Spherical valve



## Bibliography

- [1] White, F.M., 2001. *Fluid Mechanics*. 4th ed, p. 357. New York: McGraw-Hill
- [2] White, F.M., 2006. *Viscous fluid flow*. 3rd ed, p. 424. New York: McGraw-Hill
- [3] The OpenFOAM Foundation, 2011. *2.1 Lid-driven cavity flow*. [online] Available at: <<http://www.openfoam.org/docs/user/cavity.php>> [Accessed 27 January 2013]
- [4] Wiki, n.d. *Kinematic pressure*. Available at: <[http://en.wikipedia.org/wiki/Kinematic\\_pressure#Kinematic\\_pressure](http://en.wikipedia.org/wiki/Kinematic_pressure#Kinematic_pressure)> [Accessed 27 January 2013]
- [5] Versteeg, H.K. & Malalasekera, W., 1995. *An introduction to Computational Fluid Dynamics – The Finite Volume Method*. Essex: Longman Scientific & Technical
- [6] ANSYS, Inc., 2009. *7.3.2 Using Flow Boundary Conditions*. [online] Available at: <<http://www.sharcnet.ca/Software/Fluent12/html/ug/node238.htm>> [Accessed 26 May 2013]
- [7] Maji, P.K. & Biswas, G., 1999. *Analysis of flow in the spiral casing using a streamline upwind Petrov Galerkin method*. [online] <[http://onlinelibrary.wiley.com/doi/10.1002/\(SICI\)1097-0207\(19990520\)45:2%3C147::AID-NME581%3E3.0.CO;2-G/pdf](http://onlinelibrary.wiley.com/doi/10.1002/(SICI)1097-0207(19990520)45:2%3C147::AID-NME581%3E3.0.CO;2-G/pdf)> [Accessed 24 May 2013]
- [8] Nilsson, et al. (2003). *Assessment of turbulence modeling for CFD simulations into hydroturbines: Spiral casings*. [online] <[http://www.tfd.chalmers.se/~hani/postscript\\_files/CaixaEspiral2.pdf](http://www.tfd.chalmers.se/~hani/postscript_files/CaixaEspiral2.pdf)> [Accessed 4 June 2013]
- [9] Hambric, S.A., et al., 2010. Structure- and fluid-borne acoustic power sources induced by turbulent flow in 90 degree piping elbows. [online] Available at: <<http://www.sciencedirect.com/science/article/pii/S0889974609001212>> [Accessed 5 June 2013]
- [10] Drtina, P. & Sallaberger, M., 1999. *Hydraulic turbines – basic principles and state-of-the-art computational fluid dynamics applications*. [online] <<http://mecanica.eafit.edu.co/~mgarcia/mg/projects/difranco/papers-turbine/hydraulic-turbines-drtina.pdf>> [Accessed 6 June 2013]

- [11] Chapallaz, J.M., Eichenberger, P. & Fischer, G., 1992. *Manual on Pumps Used as Turbines. Appendix B: Basic theory of hydraulic machines*. [online] Available at: <<http://www.nzdl.org/gsdmod?e=d-00000-00---off-0hdl--00-0----0-10-0---0---0direct-10---4-----0-11--11-en-50---20-about---00-0-1-00-0-0-11-1-0utfZz-8-00&a=d&c=hdl&cl=CL1.11&d=HASH011f05bf8734d88d1a080257.14.2>> [Accessed 6 June 2013]
- [12] Hovland, J.M., 2013. *Pressure pulsations and stress in a high head Francis model turbine*. [mail] (Personal communication, 10 June 2013).
- [13] Kjølle, A., 2003. *Hydraulisk måleteknikk*. 2. utgave. Vannkraftlaboratoriet: NTNU
- [14] Klemetsen, L.E., 2010. *An experimental and numerical study of the free surface Pelton bucket flow*. Trondheim: NTNU
- [15] Slater, J.W., 2008. *NPARC Alliance CFD Verification and Validation Web Site*. [online] <<http://www.grc.nasa.gov/WWW/wind/valid/tutorial/valassess.html>>
- [16] Nielsen, T.K., 2013. *The influence of valve geometries on spiral casing flow conditions*. [conversation] (Personal communication, April 2013)
- [17] Electrical engineering courses, 2011. *The Pitot tube*. [JPEG] Available at: <<http://4.bp.blogspot.com/-XCTZ9KUc8SY/ULeeGnz6zaI/AAAAAAAAABjM/s40UHG2R0Sg/s1600/The+Pitot+tube.jpg>> [Accessed 10 June 2013]
- [18] Docstoc, 2011. *Hot wire/hot film anemometer*. [PNG] Available at: <[www.google.no/url?sa=i&source=imgres&cd=&cad=rja&docid=2XHmC\\_Bx8pM8mM&tbid=51pavXE69jc76M:&ved=0CAkQjBwwAA&url=http%3A%2F%2Fimg.docstocdn.com%2Fthumb%2Forig%2F53874958.png&ei=pAe2UeGxJMyJhQess4HwBQ&psig=AFQjCNGhK\\_1kK14GCji0NgAl03RCIIrUBA&ust=1370970404675359](http://www.google.no/url?sa=i&source=imgres&cd=&cad=rja&docid=2XHmC_Bx8pM8mM&tbid=51pavXE69jc76M:&ved=0CAkQjBwwAA&url=http%3A%2F%2Fimg.docstocdn.com%2Fthumb%2Forig%2F53874958.png&ei=pAe2UeGxJMyJhQess4HwBQ&psig=AFQjCNGhK_1kK14GCji0NgAl03RCIIrUBA&ust=1370970404675359)> [Accessed 10 June 2013]
- [19] Nielsen, T.K., 2012. *PPT slides "Valves" from course TEP4200*. [PDF] Trondheim: NTNU

# Appendix A: Calculations involved in a bend mesh creator for OpenFOAM's blockMeshDict

## Introduction

OpenFOAM's blockMeshDict is a very flexible tool when it comes to creating a mesh of a desired geometric mesh, while also allowing to effectively adjust the number of cells and cell distributions at various locations in the mesh. However, the disadvantage of the current blockMeshDict setup is that it is very time consuming to create a mesh of a 3D bend, as it requires plotting the position of at least 36 points in an orthogonal coordinate system, which furthermore require performing at least 13 trigonometrical calculations, before putting the resulting values into order. The purpose of this appendix is to explain how all of the required calculations are carried out, in order to create a blockMeshDict of 3D bend of any angle between 0 and 90 degrees, solely by choosing 5 input parameters: bend radius  $R$ , conduit diameter  $d$ , bend angle  $\phi$ , downstream conduit length  $L_{down}$  and upstream conduit length  $L_{up}$ .

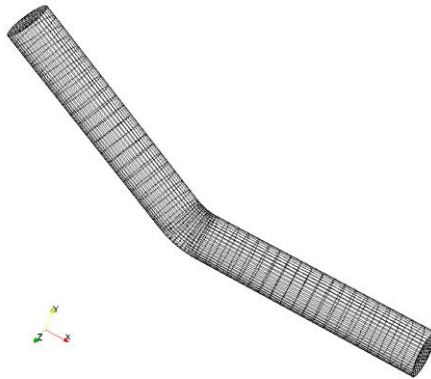


*Figure A1: A 3D 30-degree bend mesh created in blockMeshDict, featuring a relative radius  $R/r=1.5$ , and 5000 cells*

## The placement of the mesh in the coordinate system

We start out by defining our Cartesian coordinate system such that the bend outlet cross-section is located in the  $yz$  plane at  $x=0$ . The downstream conduit is parallel to the  $x$  axis, such that the mesh outlet cross-section is located in the  $yz$  plane at  $x=L_{down}$ . Furthermore, the rotational point of our bend radius will be set as the origin of our Cartesian coordinate system. If we carry on by defining the our conduit radius  $r=d/2$ , and choose that the downstream conduit will be constrained by the the boundaries  $R - r \leq y \leq R + r$  and  $-r \leq z \leq r$ . For simplicity and convenience, each of the 8 vertices defining the downstream conduit will have an angle of 45 degrees measured in the  $yz$  plane, relative to the center of the downstream conduit. This leaves us with sufficient information to define all of the vertices of the mesh outlet and the bend outlet:

## Calculating vertice coordinates

### Mesh

				outlet
$(x=L_{down}$	$y = -R - r/\sqrt{2}$	$z = -r/\sqrt{2})$	//0	Lower-z
$(x=L_{down}$	$y = -R - r/\sqrt{2}$	$z = r/\sqrt{2})$	//1	Lower+z
$(x=L_{down}$	$y = -R + r/\sqrt{2}$	$z = r/\sqrt{2})$	//2	Upper+z
$(x=L_{down}$	$y = -R + r/\sqrt{2}$	$z = -r/\sqrt{2})$	//3	Upper-z

### Bend outlet

$(x=0$	$y = -R - r/\sqrt{2}$	$z = -r/\sqrt{2})$	//4	Lower-z
$(x=0$	$y = -R - r/\sqrt{2}$	$z = r/\sqrt{2})$	//5	Lower+z
$(x=0$	$y = -R + r/\sqrt{2}$	$z = r/\sqrt{2})$	//6	Upper+z
$(x=0$	$y = -R + r/\sqrt{2}$	$z = -r/\sqrt{2})$	//7	Upper-z

### Bend inlet

For these vertices, note that  $\theta$  is our bend angle.

$(x = (-R - r/\sqrt{2}) \sin \phi$	$y = (-R - r/\sqrt{2}) \cos \phi$	$z = -r/\sqrt{2})$	//8	Lower-z
$(x = (-R - r/\sqrt{2}) \sin \phi$	$y = (-R - r/\sqrt{2}) \cos \phi$	$z = r/\sqrt{2})$		

$$\begin{aligned}
 //9 & & & \text{Lower+z} \\
 (x = (-R + r/\sqrt{2}) \sin \phi & \quad y = (-R + r/\sqrt{2}) \cos \phi & \quad z = r/\sqrt{2}) \\
 //10 & & & \text{Upper+z} \\
 (x = (-R + r/\sqrt{2}) \sin \phi & \quad y = (-R + r/\sqrt{2}) \cos \phi & \quad z = -r/\sqrt{2}) \\
 //11 & \text{Upper-z}
 \end{aligned}$$

### Mesh inlet

For these vertices, note that  $L_{up}$  is our upstream conduit length.

$$\begin{aligned}
 (x = (-R - r/\sqrt{2}) \sin \phi - L_{up} \cos \phi \\
 y = (-R - r/\sqrt{2}) \cos \phi + L_{up} \sin \phi & \quad z = -r/\sqrt{2}) \quad //12 \quad \text{Lower-z}
 \end{aligned}$$

$$\begin{aligned}
 (x = (-R - r/\sqrt{2}) \sin \phi - L_{up} \cos \phi \\
 y = (-R - r/\sqrt{2}) \cos \phi + L_{up} \sin \phi & \quad z = r/\sqrt{2}) \quad //13 \quad \text{Lower+z}
 \end{aligned}$$

$$\begin{aligned}
 (x = (-R + r/\sqrt{2}) \sin \theta - L_{up} \cos \theta \\
 y = (-R + r/\sqrt{2}) \cos \theta + L_{up} \sin \theta & \quad z = r/\sqrt{2}) \quad //14 \quad \text{Upper+z}
 \end{aligned}$$

$$\begin{aligned}
 (x = (-R + r/\sqrt{2}) \sin \theta - L_{up} \cos \theta \\
 y = (-R + r/\sqrt{2}) \cos \theta + L_{up} \sin \theta & \quad z = -r/\sqrt{2}) \quad //15 \quad \text{Upper-z}
 \end{aligned}$$

### Setting blocks

```

hex (0 1 2 3 4 5 6 7)
hex (4 5 6 7 8 9 10 11)
hex (8 9 10 11 12 13 14 15)

```

### Calculating arc coordinates

Mesh		outlet		arcs
arc 0 1	$(x=L_{down} \quad y = -R - r$	$z = 0)$	//Lower	
arc 1 2	$(x=L_{down} \quad y = -R$	$z = r)$	//Middle	
arc 2 3	$(x=L_{down} \quad y = -R + r$	$z = 0)$	//Upper	
arc 3 0	$(x=L_{down} \quad y = -R$	$z = -r)$	//Middle	

**Bend outlet arcs**

arc 4 5 ( $x=0$ )	$y = -R - r$	$z = 0$	//Lower
arc 5 6 ( $x=0$ )	$y = -R$	$z = r$	//Middle
arc 6 7 ( $x=0$ )	$y = -R + r$	$z = 0$	//Upper
arc 7 4 ( $x=0$ )	$y = -R$	$z = -r$	//Middle

**Bend arcs**

arc 4 8	$(x = (-R - r/\sqrt{2})\sin(\theta/2)$	$y = (-R - r/\sqrt{2})\cos(\theta/2)$	
	$z = -r/\sqrt{2})$	//Lower	
arc 5 9	$(x = (-R - r/\sqrt{2})\sin(\theta/2)$	$y = (-R - r/\sqrt{2})\cos(\theta/2)$	
	$z = r/\sqrt{2})$	//Middle	
arc 6 10	$(x = (-R + r/\sqrt{2})\sin(\theta/2)$		
	$y = (-R + r/\sqrt{2})\cos(\theta/2)$	$z = r/\sqrt{2})$	//Upper
arc 7 11	$(x = (-R + r/\sqrt{2})\sin(\theta/2)$		
	$y = (-R + r/\sqrt{2})\cos(\theta/2)$	$z = -r/\sqrt{2})$	//Middle

**Bend inlet arcs**

arc 8 9	$(x = (-R - r)\sin\theta$	$y = (-R - r)\cos\theta$	
	$z = 0)$	//Lower	
arc 9 10	$(x = -R\sin\theta$	$y = -R\cos\theta$	
	$z = r)$	//Middle	
arc 10 11	$(x = (-R + r)\sin\theta$	$y = (-R + r)\cos\theta$	
	$z = 0)$	//Upper	
arc 11 8	$(x = -R\sin\theta$	$y = -R\cos\theta$	
	$z = -r)$	//Middle	

**Mesh inlet arcs**

arc 12 13	$(x = (-R - r)\sin\theta - L_{\text{up}}\cos\theta$	$y = (-R - r)\cos\theta +$	
$L_{\text{up}}\sin\theta$	$z = 0)$	//Lower	
arc 13 14	$(x = -R\sin\theta - L_{\text{up}}\cos\theta$	$y = -R\cos\theta + L_{\text{up}}\sin\theta$	
	$z = r)$	//Middle	
arc 14 15	$(x = (-R + r)\sin\theta - L_{\text{up}}\cos\theta$	$y = (-R + r)\cos\theta +$	
$L_{\text{up}}\sin\theta$	$z = 0)$	//Upper	
arc 15 12	$(x = -R\sin\theta - L_{\text{up}}\cos\theta$	$y = -R\cos\theta + L_{\text{up}}\sin\theta$	
	$z = -r)$	//Middle	